Segmental Organization, Projection Identity, and Functional Recruitment of Ventral V3 Interneurons in the Adult Lumbar Spinal Cord

by

Mary Ifeakandu

A Thesis submitted to the Faculty of Graduate and Postdoctoral Studies of
The University of Manitoba
In partial fulfillment of the requirements of the degree of

MASTER OF SCIENCE

Physiology and Pathophysiology
University of Manitoba
Winnipeg

Abstract

V3 neurons are a genetically defined population of excitatory Sim1-expressing spinal INs that contribute to locomotor stability, motor coordination, and spinal motor circuit function. Although ventromedial ($V3_{VM}$) and ventrolateral ($V3_{VL}$) V3 subpopulations have been identified with distinct functions, their segmental organization, projection-associated molecular diversity, and functional recruitment in the adult lumbar spinal cord remain poorly understood. This study investigated these characteristics in adult mice. Using Sim1CreTdTomato mice, $V3_{VM}$ and $V3_{VL}$ were mapped within lumbar segments L1-L6 based on their anatomical positions in the ventral horn. Expression of the transcription factors Zfhx3 and NFIB was examined in the rostral (L2) and caudal (L6) segments as markers of putative long- and short-range projection phenotypes. Functional recruitment was assessed using cFos immunoreactivity after in vivo stimulation of the L2 or L6 ventral roots. A reproducible rostrocaudal distribution pattern was identified. $V3_{VM}$ neurons predominated throughout the lumbar spinal cord, representing 80% of ventral V3 (V3V) neurons in L1-L2, 92% in L3-L5, and 62% in L6. In contrast, $V3_{VL}$ neurons were present in the rostral lumbar, relatively sparse within the mid-lumbar enlargement, but increased significantly in the caudal lumbar cord, comprising 20.3%, 7.7%, and 37.3% of V3V neurons in L1-L2, L3-L5, and L6, respectively (n = 3 mice). Molecular analyses demonstrated that both $V3_{VM}$ and $V3_{VL}$ populations expressed Zfhx3 and NFIB, suggesting molecular heterogeneity within V3V neurons (n = 2 mice). Functional analyses revealed segment-dependent recruitment following motor pathway activation. L2 ventral root stimulation recruited $V3_{VM}$ and $V3_{VL}$ neurons similarly (52.0% and 55.5%, respectively), whereas L6 stimulation preferentially activated $V3_{VM}$ neurons (74.0%) compared with $V3_{VL}$ neurons (43.5%) (n = 5 mice). cFos expression extended into adjacent lumbar and sacral segments and was observed bilaterally, suggesting involvement of V3V neurons in intersegmental and commissural spinal networks. These findings suggest that V3V neurons exhibit spatial, molecular, and functional specialization along the rostrocaudal axis, providing insight into the organization of spinal motor circuits.

Acknowledgements

I would like to thank my supervisor, **Dr. Jeremy Chopek**, for his guidance, mentorship, patience, and support throughout my studies, all of which were instrumental in completing this work. Thank you for the support that extended beyond the academic walls, especially during the birth of my first child. Your understanding, encouragement, and kindness during that important period of my life meant more than words can adequately express. I am also grateful to my committee members, **Drs. Kristine Cowley and Katinka Stecina** for their valuable feedback, discussions, and constructive suggestions, which have strengthened both this research and my scientific growth. Katinka, I truly appreciate your support, mentorship, and belief in me, even during times when I was overwhelmed juggling my studies and family responsibilities. You have a rare gift of making complex things simple, and I am incredibly grateful for your encouragement and guidance throughout this journey. Kris, your intellectual curiosity and perspective in transforming seemingly simple observations into a deeper inquiry and understanding have challenged me to think more critically in research. Thank you for teaching me to look beyond the obvious.

I am grateful to everyone in the Chopek's Laboratory for their support. **Shannon**, thank you for your support with my experiments. Beyond lab work, I cherished the many conversations we shared, from science to movies and everything in between. It was truly a pleasure working alongside you. **Narjes**, thank you for your technical support and help whenever needed. **Camila**, thank you for being such a supportive senior colleague. I always appreciated your willingness to answer questions and provide guidance whenever I reached out. I am also grateful to the members of Nagy's lab, **Prabhisha** and **Bruce**, for access to the microscope and assistance with imaging. Thanks to my former lab members, **Muniza**, **Victoria, and Lucia,** for your support, encouragement, and kindness within and beyond the laboratory.

Special thanks to the faculty, staff, and administrative personnel of the Department of Physiology and Pathophysiology and the Spinal Cord Research Centre at the University of Manitoba for their support and academic development throughout my graduate training. I am grateful and acknowledge the financial support provided by the University of Manitoba, the Faculty of Graduate Studies, and the various scholarships, awards, and funding opportunities that supported my research and academic training and enabled me to successfully complete this work.

To my beloved family, words cannot express my gratitude. To my husband, thank you for your support, encouragement, sacrifices, and belief in me. This journey would not have been possible without you. To my children, thank you for the many sacrifices you made and for the moments we missed together while I pursued excellence in my studies. You have been a constant source of motivation and joy. To my parents and siblings, thank you for your love, prayers, and support. Your encouragement sustained me throughout this journey. Mom, I am especially grateful for your sacrifice in coming to help care for my children after I gave birth so that I could continue my studies. Your love and selflessness will never be forgotten.

Finally, I thank my mentor (**Dr Jude Uzonna**), colleagues, and friends who contributed directly or indirectly to this work. Your support, encouragement, and contributions have played an important role in bringing this thesis to completion.

Dedication

To God Almighty, whose grace, wisdom, and faithfulness sustained me throughout this journey. Through every challenge, uncertainty, and triumph, His strength carried me forward and made this achievement possible.

To my husband, Chigozie, and my Children, Chikaima, Kachiside and Chikamso.

To my parents and siblings, whose love, sacrifices, encouragement, and belief in me have been a constant source of motivation.

To all young women and mothers who dare to pursue knowledge, make an impact and advance in life despite obstacles. May this work serve as a reminder that perseverance, resilience, and faith can transform challenges into opportunities and dreams into reality.

Table of Contents

List of Tables

List of Figures

List of Acronyms/Abbreviations

A647 (Alexa Fluor 647)

AF488 (Alexa Fluor 488)

cFos (Cellular Fos Proto-Oncogene)

CPG (central pattern generator)

Cy3 (Cyanine 3)

DsRed (Discosoma Red Fluorescent Protein)

FITC (Fluorescein Isothiocyanate)

IHC (immunohistochemistry)

IN (Interneuron)

NFIB (Nuclear Factor I B)

Nkx2.2 (NK2 Homeobox 2)

PBS (phosphate-buffered saline)

PBS-T (phosphate-buffered saline – Triton)

PFA (paraformaldehyde)

RT (room temperature)

SC (spinal cord)

SCI (spinal cord injury)

Sim1 (Single-minded homolog 1)

V3V (ventral V3)

$V3_{VM}$ (ventromedial V3)

$V3_{VL}$ (ventrolateral V3)

VGlut2 (vesicular glutamate transporter 2)

Zfhx3 (Zinc Finger Homeobox 3)

Chapter I: Introduction

The spinal cord contains an intrinsic neural system capable of generating rhythmic locomotor activity even when sensory and descending inputs are removed. This phenomenon was first demonstrated in classic experiments where supraspinal and afferent inputs were severed in cats, yet locomotor-like activity with coordinated flexor–extensor alternation still emerged (Brown, 1911; Brown, 1914). Similar findings in isolated rodent spinal cords further confirmed that rhythmic patterns can arise in the absence of supraspinal input, where *in vitro* neonatal preparations produced fictive locomotion without brain influence (Kudo & Yamada, 1987; Cazalets et al., 1992; Cowley & Schmidt, 1997). These studies established the spinal central pattern generators (CPG) as an autonomous rhythm-generating circuit, a concept now well supported across vertebrate species (Grillner, 1985).

Although the CPG can generate basic rhythmic output intrinsically, sensory afferents are essential for producing smooth, stable, and adaptive locomotor behaviour (Pearson, 2004; Rossignol et al., 2006; Kiehn, 2016). Studies in spinalized cats demonstrated that removing cutaneous afferents severely impaired plantar foot placement and hindlimb weight-bearing. Partial denervation allowed recovery with training, whereas complete denervation prevented recovery despite prolonged intervention (Bouyer & Rossignol, 2003a; Varejão & Filipe, 2007). Similar instability and altered gait patterns are seen in individuals with peripheral neuropathy affecting cutaneous afferents (Lin & Yang, 2011). Sensory feedback becomes especially important during unexpected perturbations, such as stepping on an obstacle or encountering uneven terrain, where cutaneous input adjusts ongoing movements (Wutzke et al., 2013).

Descending motor control also shapes the output of spinal circuits. These signals converge in the medullary reticular formation, a major relay that transmits signals from upper motor centers to spinal networks (Brownstone & Chopek, 2018). Reticulospinal neurons receive motor-related input and project through the ventrolateral funiculus to spinal interneurons (INs) and motoneurons (Peterson, 1979; Matsuyama et al., 2004; Brownstone & Chopek, 2018). Classical stimulation studies have demonstrated that distinct dorsoventral regions of the reticular formation can activate or inhibit extensor muscles, highlighting its role in posture and locomotion (Mori, 1987).

Advances in genetics and optogenetics have further expanded our understanding of CPG organization. Genetically defined IN classes contribute to rhythm generation, left–right alternation, and pattern formation (Kiehn, 2006, 2016). Within this network, V3 neurons form a major excitatory component. They are primarily commissural and enhance the robustness and stability of rhythm, particularly when sensory feedback or locomotor demands change (Danner et al., 2019).

The spinal cord demonstrates a clearly defined rostrocaudal functional structure, wherein the rostral lumbar segments are primarily linked to the control of proximal muscles, while the caudal segments are associated with distal limb movements (Kiehn, 2016). This segmental specialization indicates that the distribution of IN populations may also be region-specific, facilitating varied motor outputs (Kiehn, 2016; Gosgnach et al., 2017). Although numerous studies have established a role for V3 neurons in coordinating locomotion and stabilizing rhythmic motor outputs (Zhang et al., 2008; Danner et al., 2019), the spatial organization of the ventral populations along the rostrocaudal axis of the adult lumbar spinal cord needs to be assessed. Early investigations largely treated V3 neurons as a homogeneous population (Zhang et al., 2008), whereas more recent work has revealed considerable heterogeneity in their morphology and functional properties (Borowska

et al., 2013 & 2015; Blacklaws et al., 2015; Chopek et al., 2018). Despite these advances, limited attention has been given to whether distinct V3 subpopulations exhibit segment-specific distribution patterns along the lumbar spinal cord.

Ventral V3 (V3V) neurons have been identified and analyzed in the low thoracis and upper lumbar spinal cord as one of the functional subpopulations of V3 neurons (Borowska et al., 2013). These studies also observed distinct intrinsic properties and spatial distribution patterns, which support their involvement in locomotor stability and commissural drive (Borowska et al., 2013; Blacklaws et al., 2015). This population was further classified into subpopulations by Chopek et al. (2018), where they demonstrated that V3V neurons segregate into functionally distinct medial and lateral populations with divergent intrinsic and circuit properties. However, a systematic, quantitative assessment of their distribution across lumbar segments has not been investigated. Determining whether these subpopulations follow a segmental gradient is essential for linking their anatomical organization to functional specialization within spinal locomotor circuits. This thesis begins to address these neuroanatomical questions

Chapter II

2.1 Spinal Motor Circuits and IN Organization

2.1.1 Overview of Spinal INs and Propriospinal Organization

Spinal INs play a central role in coordinating, refining, and adapting movement (Goulding, 2009; Kiehn, 2016; Gosgnach et al., 2017). Their ability to integrate sensory information, intrinsic rhythm-generating signals, and descending motor commands makes them essential for smooth and flexible motor control (Goulding, 2009). This functional versatility stems from the extensive diversity of IN types in the spinal cord, which differ in molecular identity, projection patterns, neurotransmitter phenotypes, physiology, and developmental origin (Gosgnach et al., 2017; Goulding, 2009). During development, distinct IN classes arise from defined progenitor domains and assemble into organized circuits that mature into robust sensorimotor networks capable of adapting to changes in speed, posture, and sensory input (Deska-Gauthier & Zhang, 2019).

Propriospinal INs expand the integrative capacity of the spinal cord by linking multiple spinal segments through short- and long-range projections. These neurons form longitudinal networks that distribute locomotor commands along the rostrocaudal axis, enabling coordination of motor output across different spinal levels (Flynn et al., 2011; Laliberte et al., 2019). Experimental studies in *in vitro* spinal cord preparations have demonstrated that propriospinal circuits can generate and sustain rhythmic locomotor-like activity in the absence of supraspinal input, highlighting their fundamental role in organizing motor output (Atsuta et al., 1991; Whelan et al., 2000; Hägglund et al., 2010). In addition to supporting intrinsic rhythm generation, propriospinal pathways contribute to the transmission of descending motor commands and coordination of multi-joint movements across spinal segments (Cowley & Schmidt, 1997; Cowley et al., 2008; Flynn et al., 2011). This longitudinal organization is particularly important in the

lumbar spinal cord, where segmental specialization underlies the control of proximal and distal limb musculature (Kiehn, 2016). Collectively, these findings emphasize that spinal INs function as an interconnected network that integrates intrinsic rhythmic activity with intersegmental coordination. Within this framework, excitatory IN populations with commissural and propriospinal projection patterns play a key role in stabilizing and distributing locomotor output across segments (Zhang et al., 2008; Chopek et al., 2018; Danner et al., 2019). The development of various types of INs has provided deep insight into these systems, using techniques such as electrophysiology, behavioural output, and protein expression. So far, over 20 IN types in the spinal cord have been identified and categorized by function.

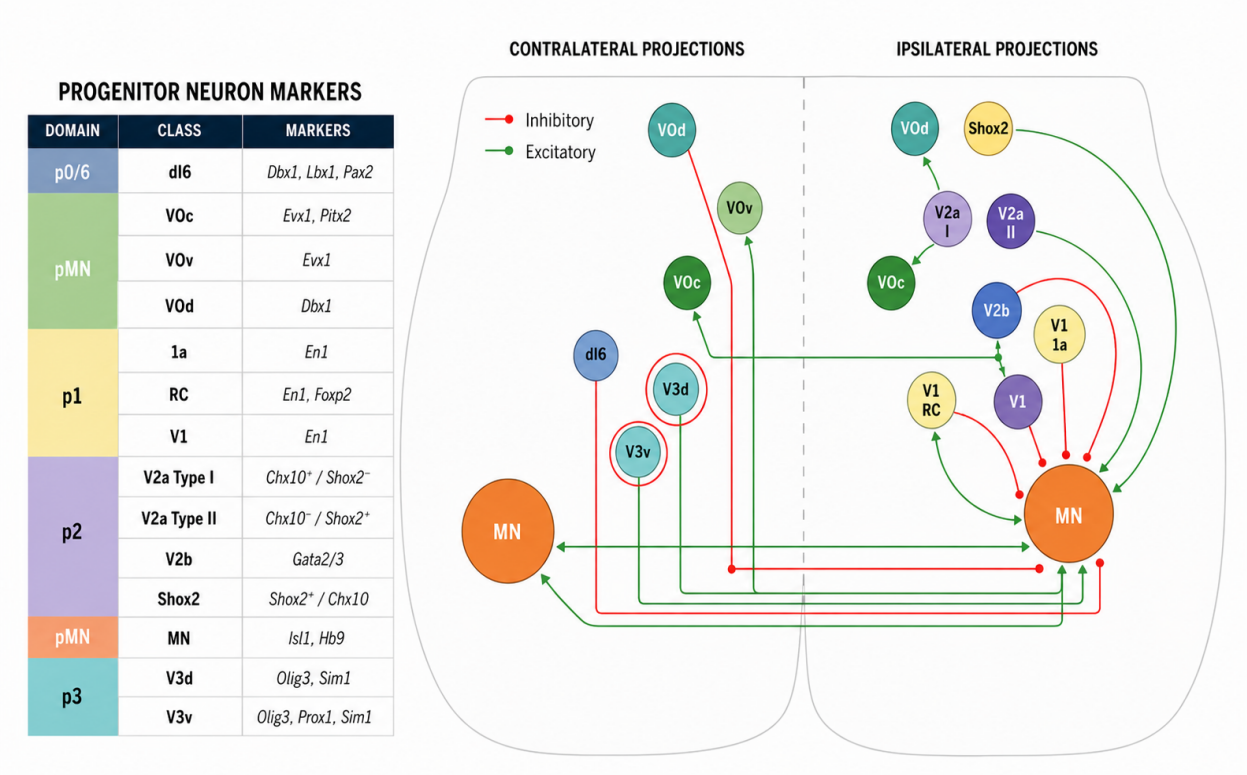

Figure 1: Overview of spinal IN circuitry with emphasis on V3 INs.
Schematic representation of spinal cord motor circuitry illustrating ipsilateral and contralateral interneuronal connections. V3 neurons (circled in red) are shown as excitatory commissural neurons projecting across the midline to influence contralateral motoneuron (MN) activity. INs within this network are classified based on neurotransmitter phenotype and projection pattern,

including excitatory glutamatergic populations (e.g., V2a), inhibitory GABAergic/glycinergic populations (e.g., V2b), and cholinergic INs. Functionally, distinct IN classes contribute to different aspects of locomotor control, with V1 neurons implicated in left–right alternation and V3 neurons contributing to rhythm stabilization and coordination. *Adapted from Jensen et al. (2020).*

2.1.2 Motoneurons as the final common pathway for spinal motor output

Motoneurons serve as the essential final conduit through which spinal circuits orchestrate movement. They integrate converging inputs from descending pathways, sensory afferents, and spinal INs, translating this synaptic convergence into muscle contractions (Sherrington, 1906; Kiehn, 2016). Within the ventral horn of the spinal cord, motoneurons are grouped into motor pools that innervate distinct muscle groups, enabling the spinal cord to produce coordinated movements of both proximal and distal limbs (McHanwell & Biscoe, 1981; Romanes, 1964; Jessell, 2000; Kandel et al., 2021). This structural organization is particularly crucial in the lumbar spinal cord, where motor pools associated with hindlimb muscles are distributed across various lumbar segments and are modulated by local networks of premotor INs (Kiehn, 2016).

V3 neurons play a key role within this premotor framework. Pioneering studies have shown that V3 neurons provide excitatory input to motoneurons and other premotor INs such as, establishing their function as an excitatory foundation for consistent locomotor output (Zhang et al., 2008). More recent findings indicate that V3 neurons have a broad innervation profile of motoneurons and can rapidly modulate bilateral motor output, underscoring their importance in activating motor pools and coordinating spinal motor activity (Zhang et al., 2025). Thus, investigating the distribution and recruitment of V3 subpopulations in relation to segmental motor outputs can enhance our understanding of how spinal circuits regulate hindlimb movements.

2.1.3 Segmental organization of the lumbar spinal cord and relevance to V3 subpopulation mapping

The spinal cord exhibits segmental organization, with each segment regulating specific body regions through its motoneurons, sensory inputs, and Interneuronal networks (Kandel et al., 2021). In mice, the spinal cord comprises six lumbar segments, and the lumbar enlargement houses the circuits essential for controlling hindlimb movement. Anatomically and functionally, the lumbar segments differ; the rostral and caudal regions have distinct contributions to locomotion and limb movement (Cazalets et al., 1995; Kiehn, 2016; Rybak et al., 2015).

Typically, the rostral lumbar segments are linked to the activation of proximal hindlimb muscles, while the more caudal lumbar segments are involved in controlling distal hindlimb actions (Romanes, 1964; McHanwell & Biscoe, 1981). This rostrocaudal functional differentiation is crucial for analyzing the distribution of INs. If motor control is organized by segment, then the premotor INs populations that facilitate locomotor stability and coordination might also reflect this segment-specific organization. This concept is particularly pertinent to V3V neurons, as demonstrated by Chopek et al. (2018), who categorized them into ventromedial ($V3_{VM}$) and ventrolateral ($V3_{VL}$) groups with distinct circuit characteristics. $V3_{VM}$ neurons were found to participate in recurrent excitatory networks with other V3 INs, suggesting a role in amplifying and integrating excitatory drive within spinal locomotor circuits. In contrast, $V3_{VL}$ neurons formed direct excitatory synaptic connections with ipsilateral motoneurons, indicating a more prominent role in premotor output and the direct regulation of motor activity (Chopek et al., 2018). However, the question of whether these subpopulations are uniformly distributed across the lumbar segments or exhibit rostrocaudal variation has yet to be systematically explored. Conducting a mapping of $V3_{VM}$ and $V3_{VL}$ neurons across L1–L6 is essential for establishing a foundational anatomical understanding of how these subpopulations may influence segment-specific motor control.

2.2 V3 Neurons

2.2.1 V3 Neurons in Locomotor Circuit Function

V3 neurons are derived from Nkx2.2-positive p3 progenitors and are identified by the expression of the transcription factor Sim1. During development, V3 neurons migrate to ventral lamina IV, V, VI, VII and VIII, where they differentiate into glutamatergic INs with predominantly commissural axons, and a small subset with ipsilateral or bilateral projections (Zhang et al., 2008; Goulding, 2009). Reporter and in situ studies show that V3 neurons selectively express the vesicular glutamate transporter VGlut2, with no markers of inhibitory or cholinergic phenotypes, indicating that this population comprises exclusively excitatory INs (Zhang et al., 2008).

Using Sim1Cre-dependent axonal reporters and VGLUT2 immunohistochemistry, Zhang and colleagues quantified V3-derived glutamatergic boutons on ventral horn neurons. They showed that V3 neurons form dense excitatory synaptic contacts onto motoneurons, Ia inhibitory INs, Renshaw cells, V2 (Lhx3+) neurons, and lamina VIII commissural INs, contributing roughly 22–27 percent of the VGLUT2-positive inputs to these targets (Zhang et al., 2008). These findings establish V3 neurons as a major source of premotor excitatory drive within spinal locomotor circuits.

Functional studies provide further insight into the contribution of V3 neurons to locomotor control. Conditional expression of tetanus toxin in V3 neurons, which blocks neurotransmitter release, produced unstable, asymmetric fictive locomotor rhythms in isolated neonatal spinal cords (Zhang et al., 2008). Burst durations became irregular, step-cycle timing varied markedly, and in many preparations, stable rhythm generation failed. Despite these disturbances, left–right alternation remained intact, but the duration of flexor bursts often differed between sides. Acute silencing of V3 neurons in both neonatal preparations and behavioural adult mice produced similar

disruptions in rhythmic stability. These observations indicate that V3 neurons are not core rhythm generators, instead provide distributed excitatory drive across both halves of the spinal cord, ensuring robust and balanced locomotor output (Zhang et al., 2008; Danner et al., 2019).

Computational and modelling studies further support this view. Simulations incorporating V3 connectivity suggest that these neurons facilitate excitatory coupling between flexor and extensor modules, help coordinate motor pool activation, and contribute to smooth gait transitions during changes in speed and behavioural state (Rybak et al. 2013; 2015; Shevtsova et al., 2015; Danner et al., 2016, 2017; Ausborn et al., 2021). While the downstream functions and connectivity of V3 neurons are increasingly well described, it remains unclear how V3V subpopulations are organized within this propriospinal framework. Whether ventromedial and ventrolateral V3 neurons exhibit distinct rostrocaudal distributions, differ in projection identity, or are differentially recruited during motor activation remains to be determined.

2.2.2 Dorsal V3 and Ventral V3 (V3V) Neurons

V3 neurons can be subdivided into dorsal and ventral populations based on their location, morphology, and intrinsic firing properties. Early work showed that V3V neurons are predominantly located in the ventral lamina VIII, where they exhibit relatively simple branching patterns and fast tonic firing. In contrast, dorsal V3 neurons exhibit more complex morphologies, lower average spike frequencies, and stronger spike-frequency adaptation (Goulding, 2009; Borowska et al., 2013). These differences suggest functional diversity within the broader V3 population.

Genetic studies have revealed substantial molecular heterogeneity within the V3 population. Distinct V3 subgroups can be identified by differential expression of transcription factors, including Olig3, Prox1, Bhlhb5, Nurr1, for V3V neurons, and members of the Onecut family (OC1, OC2, and OC3), for dorsal V3 neurons, which are associated with different settling positions and developmental trajectories within the spinal cord (Borowska et al., 2013; Francius et al., 2013). This molecular separation indicates that V3 neurons form distinct subpopulations with differentiated roles during circuit formation. Further refinement of the ventral population was demonstrated by Chopek et al. (2018), who identified ventromedial (VM) and ventrolateral (VL) V3 subpopulations based on soma size, location, and synaptic connectivity. In this work, $V3_{VL}$ neurons formed direct monosynaptic excitatory connections onto ipsilateral motoneurons. In contrast, $V3_{VM}$ neurons formed recurrent excitatory networks with other V3 neurons and projected to regions associated with target regions of synaptic input from descending supraspinal axons

2.2.3 V3V Neurons and Layered Microcircuit Organization

Based on their anatomical positioning and connectivity, Chopek et al. (2018) proposed a layered organization of V3V circuits, in which $V3_{VM}$ neurons form an interconnected medial network that integrates incoming signals, while $V3_{VL}$ neurons relay processed signals to specific motor pools. This arrangement is conceptually analogous to layered processing observed in other central nervous system structures, such as the neocortex, where distinct layers support intra-laminar integration, inter-laminar communication, and output-specific projection pathways (Schubert et al., 2007; Chopek et al., 2018).

Within this framework, $V3_{VM}$ neurons may function as integrative nodes, coordinating activity across spinal circuits, whereas $V3_{VL}$ neurons may contribute to the selective activation of

ipsilateral motoneurons and segment-specific motor outputs. This functional segregation suggests that spatial positioning within the ventral horn is closely linked to circuit role, with medial-lateral organization reflecting a transition from integration to output. Importantly, while this microcircuit organization has been described at the level of local connectivity, it remains unclear how these V3V subpopulations are distributed across the rostrocaudal axis of the lumbar spinal cord, whether they differ in projection identity, and how they are recruited during motor activation.

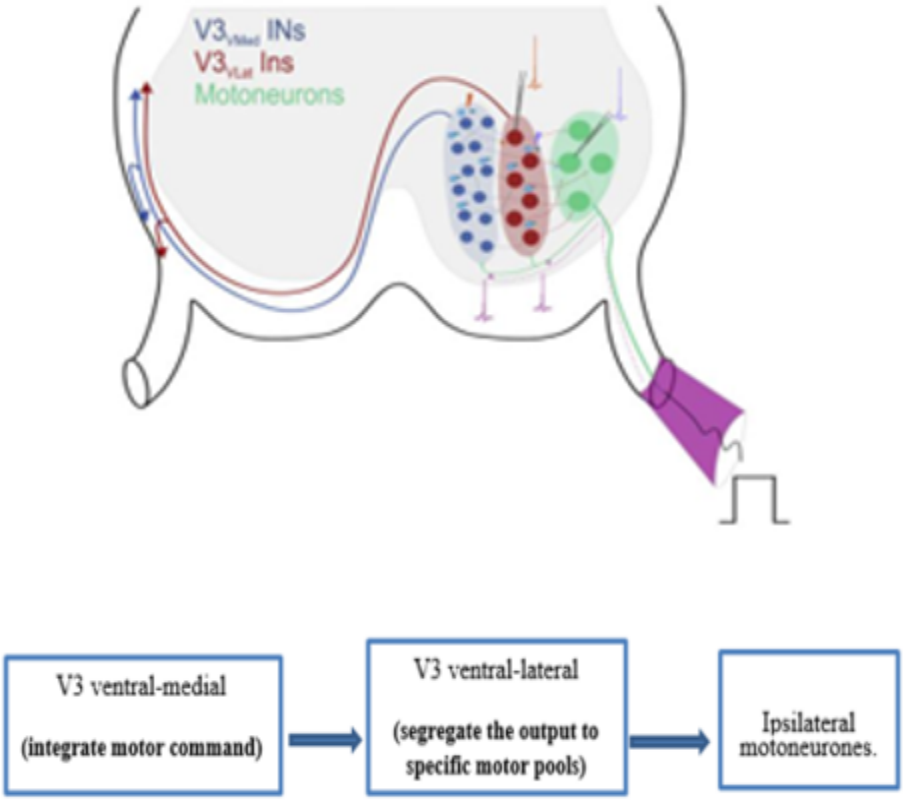

Figure 2: Local Layered V3 IN Microcircuits Involving $V3_{VM}$ INs (Blue), $V3_{VL}$ INs (Red), and MNs. Adapted from (Chopek et al., 2018)

2.2.4 Developmental Classes of Ventral Spinal INs

The ventral V-class INs include V0, V1, V2, and V3 populations, each defined by specific transcription factors expressed during development (Jessell, 2000; Alaynick et al., 2011; Francius et al., 2013). These genetically identified groups contribute distinct functions to locomotor behaviour. V0 INs regulate speed-dependent left-right alternation through inhibitory (V0D) and excitatory (V0V) subpopulations, while V0C cholinergic INs modulate motoneuron excitability (Lanuza et al., 2004; Zagoraiou et al., 2009; Talpalar et al., 2013). V1 INs comprise numerous inhibitory subclasses, including Renshaw cells and Ia inhibitory INs, which contribute to reciprocal inhibition, motor timing, and locomotor speed regulation (Gosgnach et al., 2006; Bikoff et al., 2016). V2 INs include excitatory V2a and inhibitory V2b populations that regulate gait transitions and flexor-extensor coordination (Crone et al., 2008; Zhang et al., 2014). V3 neurons, derived from the p3 domain and marked by Sim1 expression, form a major excitatory population that projects both ipsilaterally and contralaterally. Their activity contributes to left-right coordination (Zhang et al., 2008) and to the stabilization of the locomotor rhythm, especially when sensory feedback or locomotor demands change (Danner et al., 2019). This places V3 neurons at a critical node within the spinal locomotor circuitry.

A fundamental characteristic of spinal INs is their capacity to integrate supraspinal and peripheral sensory inputs (Sherrington, 1906; Baldissera et al., 1981; Jankowska, 1992, 2001). Their ability to receive convergent signals makes them key mediators of sensory-motor integration. Commissural INs, including subsets of V0 and V3 neurons, play a particularly important role in coordinating activity across body sides and distributing motor commands (Jankowska, 2008; Kiehn et al., 2008; Maxwell & Soteropoulos, 2020). Recent work demonstrates that certain descending commissural INs can be activated by supraspinal signals such as reticulospinal and

vestibulospinal input, while peripheral sensory afferents activate partially distinct populations, highlighting the complexity of the integrative spinal circuitry (Szokol et al., 2011; Kasumacic et al., 2015; LaPallo et al., 2019; Giorgi et al., 2023). V3 neurons, as a class of excitatory commissural neurons, are well-positioned within this system. Their ability to coordinate bilateral activity and influence motor output, combined with emerging evidence of anatomical and functional heterogeneity, suggests that they may contribute to both local circuit stabilization and intersegmental coordination (Zhang et al., 2008; Chopek et al., 2018; Danner et al., 2019).

2.2.5 Evolution of V3 Neuron Research: From Homogeneity to Functional Specialization

Research on spinal V3 neurons has advanced considerably over the last twenty years, evolving from their initial characterization as a singular genetically defined group to an appreciation of their functional and molecular diversity. Pioneering work by Zhang et al. (2008) identified V3 neurons as excitatory, primarily commissural neurons that are glutamatergic in spinal motor circuits, a feature vital for sustaining a stable locomotor rhythm. The genetic silencing of V3 neurons led to disrupted, asymmetric locomotion, underscoring the essential role of V3 outputs in maintaining rhythmic stability (Zhang et al., 2008). Subsequent investigations highlighted the heterogeneity of V3 neurons. Electrophysiological and morphological studies revealed distinct dorsal and V3V subpopulations, each with unique intrinsic characteristics and firing behaviours (Borowska et al., 2013; Borowska et al., 2015). V3V neurons demonstrated tonic firing patterns and were localized in the ventral laminae, suggesting a more direct role in motor output pathways.

Further insights emerged from microcircuit-level investigations, notably by Chopek et al. (2018), who identified two distinct subpopulations of V3V neurons: $V3_{VM}$ and $V3_{VL}$, differentiated

by their connectivity features. Specifically, $V3_{VL}$ neurons establish direct excitatory synapses with motoneurons, whereas $V3_{VM}$ neurons participate in recurrent excitatory networks and project to areas implicated in integrating descending inputs. This research established that the spatial arrangement within the ventral horn predicts functional circuit roles.

Recent studies have further broadened the understanding of V3 neuron functions, demonstrating their roles in long-range coordination and autonomic integration (Zhang et al., 2022; Chacon et al., 2023). Developmental investigations also indicated that the diversity of V3 neurons is influenced by temporal patterns of neurogenesis, with early-born neurons exhibiting broader projection patterns than the more confined projections of late-born neurons (Deska-Gauthier et al., 2020; 2024). Further evidence suggests functional specialization in the mature spinal cord. Here, they identified a population of V3V neurons that contribute to primary afferent depolarization (PAD), revealing a previously unrecognized role for V3 neurons in modulating sensory transmission and sensorimotor integration (Lin et al., 2023). These findings expanded the functional repertoire of V3 neurons beyond locomotor coordination and premotor excitation, demonstrating their ability to regulate sensory feedback pathways within spinal circuits (Lin et al., 2023). In addition, V3 neurons have been implicated in the pathophysiology of spasticity following spinal cord injury. Following injury, V3 neurons exhibit increased excitability, contributing to exaggerated motor output and involuntary muscle activity, suggesting that adaptive or maladaptive plasticity within V3 circuits may contribute to the development of spastic motor symptoms (Lin et al., 2019; Zhang et al., 2023). Beyond their role in sensorimotor circuitry, V3 INs likely participate in broader spinal network integration, as demonstrated by Chacon et al. (2023), who showed that lumbar V3 INs project to and provide excitatory input to thoracic sympathetic preganglionic neurons (SPNs). Collectively, these findings illustrate that V3 neurons constitute a diverse

population characterized by spatial, developmental, and functional specialization, providing a conceptual framework for further exploration of the organization, molecular characterization, and functional recruitment of adult V3V subpopulations.

2.3 Projection Identity and Organizational Diversity of V3V Neurons

2.3.1 Defining Long Vs Short Projection Markers

Transcription factors are increasingly recognized as molecular markers for identifying different types of neurons, including their projection patterns and functional roles. Studies on spinal INs have shown that distinct gene expression profiles are associated with axonal projection length and connectivity patterns (Delile et al., 2019; Bikoff et al., 2016). Here, we classify long projections as intersegmental projections spanning more than one segment, whereas short projections are classified as local connectivity within the same segment. Zfhx3 (Zinc finger homeobox 3) functions as a transcription factor involved in the maturation of neurons and the development of long-range projection characteristics in various areas of the central nervous system. Research has linked Zfhx3 to the differentiation of neurons with long axonal projections and the modulation of connectivity between neurons across distant locations (Delile et al., 2019). Its expression has been identified in multiple spinal projection-neuron populations that play a role in the long-distance coordination of motor circuits, including subsets of V2a-derived propriospinal neurons, spinocerebellar neurons, long ascending propriospinal neurons, long descending propriospinal neurons and other long-range projection neurons (Delile et al., 2019; Osseward et al., 2021), indicating its potential as a marker for neurons that project over long distances.

NFIB (Nuclear factor I/B) functions as a transcription factor, playing a crucial role in neuronal differentiation and the formation of local circuits. It has been associated with the

development of neurons characterized by more confined, short-range projection patterns and local synaptic integration (Delile et al., 2019; Hsu et al., 2015; Piper et al., 2010). Its influence on cell maturation and positioning within local circuits justifies its identification as a marker of short-range or locally projecting neuronal subtypes. The observed expression patterns were used to infer potential projection identities: neurons associated with Zfhx3 suggested long-range projection characteristics, whereas those linked to NFIB indicated short-range or local projection characteristics. This interpretation aligns with established transcriptional profiles of spinal INs subtypes (Osseward et al., 2021).

2.4 Experimental Approaches for Assessing Functional Recruitment

2.4.1 Ventral root stimulation and antidromic activation of motor pathways

Ventral roots are composed of the axonal projections of spinal motoneurons that exit the spinal cord to innervate skeletal muscles, thereby forming the final common pathway for motor output (Kandel et al., 2021; Purves et al., 2018). Electrical stimulation of a ventral root directly activates these motor axons, producing muscle contractions through orthodromic conduction toward the periphery. In addition to typical orthodromic signal propagation toward the muscle, stimulation can induce antidromic action potentials that propagate back toward the motoneuron cell bodies in the ventral horn. Antidromic activation of motoneurons via stimulation of ventral roots or peripheral motor nerves has long been a valuable experimental approach for examining motoneuron excitability, recurrent circuitry, and motor pathway organization (Eccles, 1955; Kuno, 1959; Lipski, 1981). In isolated spinal cord preparations, ventral root stimulation has been widely used to investigate spinal motor circuitry because antidromically activated motoneurons can influence local Interneuronal networks through recurrent collateral projections and interactions with premotor INs (O'Donovan et al., 1985; Mentis et al., 2005; Quinlan and Kiehn, 2007).

Consequently, ventral root stimulation provides a controlled means of activating segment-specific motor pathways while minimizing direct recruitment of sensory afferents.

In the present study, stimulating the ventral root provides a controlled means to activate specific motor pathways at specific segments. Stimulation at lumbar levels L2 or L6 is expected to activate motor axons innervating those segments, resulting in muscle contractions that confirm the accurate positioning of the stimulating electrode. Given that antidromic activity can propagate back into the ventral horn, it may engage local spinal circuits via motoneuron-related network activity and recurrent interactions with premotor segments. This interaction is particularly significant for V3 neurons, which have been shown to be connected to motoneurons and other premotor IN groups (Zhang et al., 2008; Chopek et al., 2018). Hence, the expression of cFos in response to the stimulation of L2 or L6 ventral roots is viewed as an activity-dependent indicator of spinal network engagement associated with the activation of segment-specific motor pathways. Notably, since the dorsal root was severed in this study, the observed recruitment is less likely attributable to direct sensory feedback and is more likely to reflect the activation of motor efferent pathways and related spinal circuitry.

2.4.2 Detection of Immediate Early Gene Activity Using cFos

The immediate-early gene cFos is commonly used as a marker of neuronal activation because it is rapidly transcribed in response to synaptic activity. When neurons depolarize, they activate intracellular signalling pathways that lead to cFos expression within 60–90 minutes, enabling identification of recently active neurons (Morgan & Curran, 1991; Kovács, 2008). In spinal cord research, cFos has been widely used to analyze neuronal activation during locomotion and motor activity (Morgan & Curran, 1991; Carr et al., 1995; Borowska et al., 2013). Research

has indicated that specific populations of INs, such as V3 neurons, exhibit cFos expression that depends on their activity following locomotor tasks, including treadmill running and swimming (Borowska et al., 2013). The study revealed that different subsets of V3 neurons are selectively activated during locomotion, exhibiting varied activation patterns across dorsoventral regions. This demonstrates that distinct spinal IN subtypes are differentially engaged across various motor behaviours, reinforcing the utility of cFos as an indicator of circuit engagement.

In the current study, cFos immunoreactivity was utilized to evaluate activity-dependent recruitment of V3V subpopulations following specific stimulation of the L2 and L6 ventral roots. The analysis quantified nuclear cFos expression in identified $V3_{VM}$ and $V3_{VL}$ neurons, interpreting it as an indicator of recent neuronal activation, which allowed comparison of functional engagement across segments and between medial and lateral subpopulations.

2.5 Rationale of the Study

V3 neurons are Sim1-expressing excitatory neurons derived from the p3 progenitor domain that play essential roles in locomotor stability, left-right coordination, and motor output regulation (Zhang et al., 2008; Danner et al., 2019). To further advance the study of V3 neurons, this thesis investigates the spatial organization, molecular identity, and functional recruitment of V3V neurons in the adult lumbar spinal cord to deepen our understanding of their contributions to spinal motor circuit organization. Although previous studies have demonstrated that V3V neurons comprise anatomically and functionally distinct ventromedial ($V3_{VM}$) and ventrolateral ($V3_{VL}$) populations (Chopek et al., 2018), their distribution along the rostrocaudal axis of the lumbar spinal cord has not been systematically examined. This represents an important knowledge gap because

lumbar spinal segments are functionally specialized and contribute differentially to hindlimb motor control (Kiehn, 2016).

Furthermore, emerging evidence indicates that molecular identity is closely linked to neuronal connectivity and circuit function, with transcription factors such as Zfhx3 and NFIB being associated with projection-neuron developmental programs and connectivity patterns in multiple spinal IN populations (Delile et al., 2019; Sagner et al., 2021; Osseward et al., 2021). However, it remains unknown whether V3V neurons exhibit similar projection-associated molecular heterogeneity. Likewise, although V3 neurons are recruited during motor network activity (Borowska et al., 2013), it is unclear whether functional activation differs between $V3_{VM}$ and $V3_{VL}$ populations or across lumbar segments.

Therefore, the present study seeks to address these gaps by integrating anatomical, molecular, and functional approaches to investigate V3V neurons in the lumbar spinal cord of adult mice. Specifically, this work begins to quantify the rostrocaudal distribution of ventromedial and ventrolateral V3 populations, characterizes their molecular projection identity using the transcription factors Zfhx3 and NFIB, and examines their activity-dependent recruitment following segment-specific stimulation of the L2 and L6 ventral roots. By linking spatial organization, projection-related molecular identity, and functional activation within the same neuronal population, this study aims to provide a more comprehensive understanding of the organizational principles that govern V3V neurons and their contributions to spinal motor circuit function.

2.6 Aims & Objectives

2.6.1 Overall Aim

To determine how V3V neuron subpopulations are spatially organized across the adult lumbar spinal cord, their projection-specific molecular stratification, and how they are differentially recruited following motor pathway stimulation.

2.6.2 Specific Objectives

1. **Quantify the rostrocaudal distribution** of ventromedial ($V3_{VM}$) and ventrolateral ($V3_{VL}$) V3 neurons across rostral (L1–L2), mid (L3–L5), and caudal (L6) lumbar segments.
2. **Characterize molecular projection identity** within V3V subpopulations using Zfhx3 and NFIB as markers of putative long- and short-range projection subtypes.
3. **Assess activity-dependent recruitment** of $V3_{VM}$ and $V3_{VL}$ neurons using cFos expression following L2 & L6 ventral root stimulation.

Chapter III: Methods

3.1 Ethics Declaration

All experimental protocols were approved by the Central Animal Care Committee at the University of Manitoba (protocol 23-043) prior to the commencement of the experiments and were carried out in adherence to the standards set forth by the Canadian Council on Animal Care.

3.2 Mice & Mouse Genetics

The generation and genotyping of Sim1Cre/$^{+}$ mice were performed following the procedures outlined by Zhang et al. (2008). These Sim1Cre/$^{+}$ mice were subsequently bred with TdTomato Ai9 mice (Rosa26floxstopTdTom, Jackson Laboratory) to produce Sim1Cre-tdTomato mice, which endogenously express the fluorescent protein tdTomato in Sim1Cre^{+} neuronal cell bodies, axons, and axon terminals. Both adult male and female Sim1Cre TdTom mice were used.

3.3 Tissue Sectioning

Spinal cord dura and roots were removed, and the lumbar spinal cord (L1-L6) was blocked. Tissue samples were then preserved in Tissue-Tek® O.C.T Compound (Sakura) and subsequently cryosectioned between 20 μm and 30 μm thick using a CryoStar NX50 (Thermo Scientific). Individual sections were placed on pre-cleaned Superfrost Plus microscope slides (Fisherbrand) and stored at -20° C. Sections were collected in serial order and organized into systematic sampling sets to allow unbiased rostrocaudal representation. Stained sections were placed on glass slides and covered with an appropriate mounting medium. The slides were then preserved at 4°C until imaging was conducted.

3.4 Immunohistochemistry

Spinal cord tissue sections were prepared for immunofluorescent staining to visualize subpopulations of V3V neurons, along with projection-associated markers (Zfhx3 and NFIB) and a marker of activity-dependent expression (cFos). Before staining, all sections were allowed to acclimate to room temperature for approximately 30 minutes. Following this, sections were washed in either phosphate-buffered saline (PBS; 0.1 M) or PBS supplemented with 0.2% Triton X-100 (PBST), with each wash comprising three 10-minute cycles to eliminate any remaining cryoprotectant and enhance membrane permeability.

Primary & Secondary Antibody Incubation

To minimize non-specific binding, tissue sections were treated with a blocking solution containing 10% normal donkey serum in either PBS or PBST for one hour at room temperature. After blocking, the sections were incubated with primary antibodies diluted in PBS with 1% donkey serum. This primary antibody incubation was carried out overnight at room temperature to optimize antigen-antibody interaction.

Following primary incubation, the sections were rinsed in phosphate-buffered saline (PBS) three times for 10 minutes each, then incubated with fluorescent secondary antibodies specific to the species, diluted in PBS containing 1% donkey serum. This secondary incubation lasted 2 hours at room temperature in the dark to prevent photobleaching. Following this, the sections were washed once with PBS for 10 minutes, then twice in Tris-HCl buffer, each lasting 10 minutes, to minimize background fluorescence.

Control sections, in which primary antibodies were omitted, were included to assess non-specific binding of the secondary antibodies.

Table 1: List of antibodies used for IHC protocols and their concentration.

Primaries	**Host Species**	**Concentration**	**Function**
DsRed	Mouse	1:250-1:500	V3(tdTomato) identification
NFIB	Rabbit	1:250	Short projection marker
Zfhx3	Sheep	1:100	Long projection marker
cFos	Guinea pig	1:2000	Activity-dependent marker
Secondaries			
Anti-mouse cy3	Donkey	1:250-1:500	Detect DsRed
Anti-rabbit AF488	Donkey	1:250	Detect NFIB
Anti-sheep FITC	Donkey	1:100	Detect Zfhx3
Anti-guinea pig A647	Donkey	1:500	Detect cFos

3.5. Statistical Analysis

To examine the differences between the rostral (L1-L2), mid (L3-L5), and caudal (L6) groups of $V3_{VM}$ and $V3_{VL}$ lumbar segments, soma counts were quantified for each animal. Due to the limited number of animals examined (n = 3), formal normality testing was not considered reliable, and this study was treated primarily as descriptive. Percentages of $V3_{VM}$ and $V3_{VL}$ neurons were calculated from raw soma counts for each animal to illustrate their relative medial and lateral distribution across lumbar segments. Accordingly, segmental differences are presented descriptively using both raw counts and percentages. Analyses of $NFIB^{+}$/$tdTomato^{+}$,

Zfhx3^{+}/tdTomato^{+}, and cFos+/tdTomato+ populations were likewise descriptive due to limited sample size.

3.6. Specific Methods Per Objective

3.6.1. Quantification of Rostrocaudal Distribution of $V3_{VM}$ and $V3_{VL}$_Objective 1

In each transverse section, the ventral horn was outlined using the central canal and anterior median fissure as anatomical landmarks. A mediolateral axis extending from the midline to the lateral edge of the ventral horn was then used for consistent classification. The ventral horn was divided into three equal regions, designating the medial one-third as ventromedial V3 ($V3_{VM}$) and the lateral two-thirds as ventrolateral V3 ($V3_{VL}$). This spatial classification aligns with established methodologies for medial and lateral anatomical classification of V3V subpopulations (Chopek et al., 2018).

Total counts of tdTomato-positive V3 neurons were obtained and categorized into $V3_{VM}$ and $V3_{VL}$ populations from systematically sampled sections, grouped by rostrocaudal segments: rostral (L1–L2), mid-lumbar (L3–L5), and caudal (L6). The boundaries of the lumbar segments were established using anatomical landmarks, referencing the Allen Mouse Brain Atlas (Allen Institute for Brain Science, 2011). To facilitate inter-segment and inter-Mouse comparisons, **density was calculated as the average number of V3 neuronal somata per section within each segment, accounting for variations in section sampling**. Relative proportions of $V3_{VM}$ and $V3_{VL}$ neurons were expressed as percentages of the total V3V population.

Spinal Cord Sectioning and Serial Collection

Transverse sections of the lumbar spinal cord were cut at a thickness of **20- 30 µm** using a cryostat. Sections were collected serially and distributed into **multiple sets** depending on the Mouse: Adult mice (both males (n=2) and females (n=1); aged P106–P154)

- Mouse 1: 4 serial sets (A–D), 4 blocks/set ~120 sections (30 **µm)**
- Mouse 2: 5 serial sets (A–E), 3 blocks/set ~130 sections (30 **µm)**
- Mouse 3: 5 serial sets (A–E), 5 blocks/set ~260 sections (20 **µm)**

This serial collection strategy ensured even representation of the entire rostrocaudal extent of the lumbar spinal cord.

Systematic Sampling Strategy

To achieve uniform sampling across L1–L6, sections were **systematically subsampled** from selected sets:

- Mouse 1: sections from sets C and D (n = 15)
- Mouse 2: sections from sets C and E (n = 16)
- Mouse 3: sections from sets B and D (n = 24)

Within each selected set, **every fifth section** was analyzed. With a very few exceptions (19 out of 55 sections), if the 5^{th} section is damaged, the adjacent section is selected.

This approach resulted in approximate rostrocaudal sampling intervals of:

- ~264 µm (Mouse 1)
- ~320 µm (Mouse 2)

- ~349 µm (Mouse 3)

This systematic sampling ensured representative coverage of the lumbar spinal cord while minimizing redundancy.

Microscopy & Image Analysis

Imaging for anatomical mapping and quantification of V3 neuron distribution was conducted using a Zeiss Axio Imager Z.2 upright microscope. The tdTomato^{+} V3V neurons were visualized at 10x tiled magnification (for anatomical mapping), 20x and 40x magnification (with ~8-12 Z-stacks per image) to ensure complete coverage of each section and analyzed using ZenLite software. Approximately 15-24 lumbar V3 spinal cord sections spanning L1-L6 were imaged per Mouse (n=3), across the 3 mice to derive a representative rostrocaudal distribution. Quantification was performed bilaterally across left and right ventral horn regions.

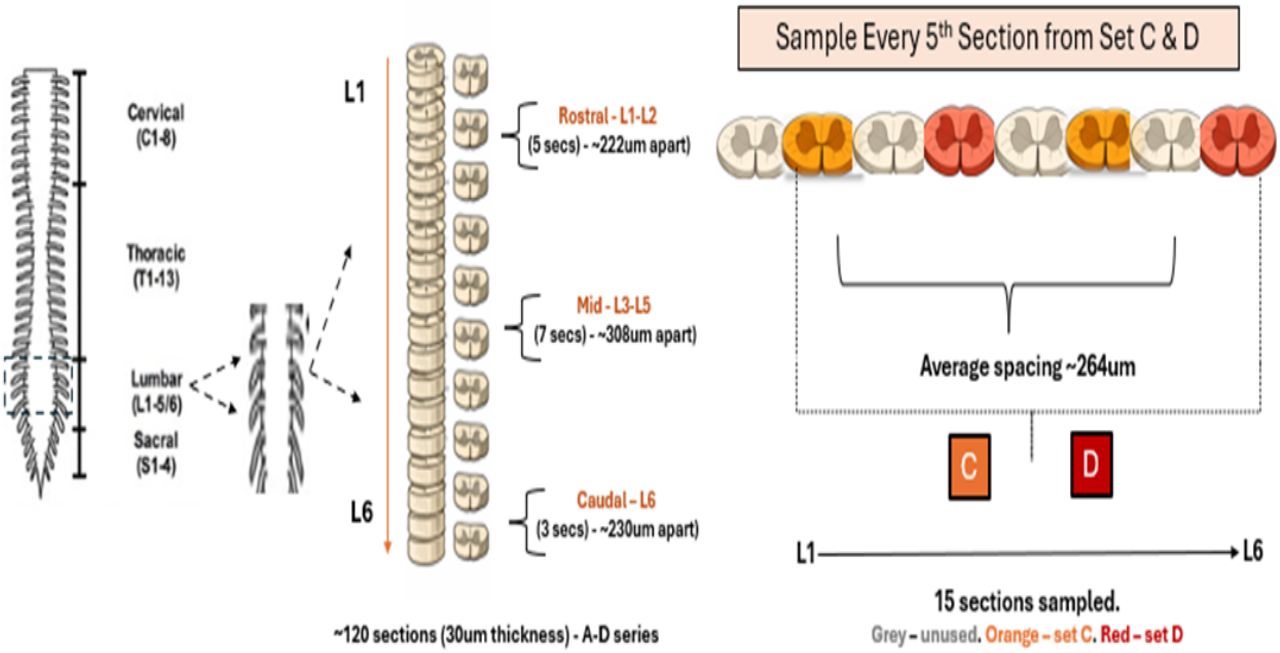

Figure 3: Sampling strategy for Lumbar Segments to assess the rostrocaudal distribution of Mouse 1. Anatomical location of lumbar spinal cord segments analyzed (L1–L6). Rostral (L1-L2 – 5 secs), mid (L3-L5 – 7 secs) and caudal (L6 – 3 secs). Transverse spinal cord sections (30 µm) were collected in four serial sets (A–D). Approximately 120 sections were obtained across the lumbar region. 15 Sections from sets C and D were systematically sampled every fifth section, resulting in an average rostrocaudal spacing of ~264 µm between analyzed sections.

3.6.2. Molecular Characterization of V3 Subpopulations (Zfhx3 & NFIB) - Objective 2

In this study, the expression of Zfhx3 and NFIB was used to determine the projection identities of various V3V neuron subpopulations. Neurons that exhibited Zfhx3 were identified as potential long-range projection neurons, whereas those expressing NFIB were potential short-range or locally projecting neurons. To investigate the projection identity of V3V subpopulations, co-expression with the transcription factors Zfhx3 or NFIB was analyzed. Each identified V3 neuron was assessed for the presence of Zfhx3 or NFIB immunoreactivity.

V3 neurons were categorized based on marker expression into three distinct groups: Zfhx3^{+}, NFIB^{+}, or negative for both. This classification was conducted separately for the ventromedial and ventrolateral populations. The analysis was confined to spinal cord segments L2 and L6, where both $V3_{VM}$ and $V3_{VL}$ subpopulations are present. This also allowed for a direct comparison between the rostral and caudal regions of the lumbar spinal cord. Quantitative analysis was reported as the percentage of NFIB or Zfhx3 in each V3 subpopulation in both the L2 and L6 segments.

Microscopy & Image Analysis

For molecular characterization of projection identity, sections were imaged with the Zeiss Axio Imager Z.2 at 10× and 40× magnification. Low magnification (10×) was used for anatomical orientation, while higher magnification (40×) with ~8–12 Z-stacks per image were used to assess marker co-localization. Double-labelled neurons, such as NFIB-A488^{+}/tdTomato^{+} or Zfhx3-FITC^{+}/tdTomato$^{+,}$ were quantified. Images were imported into IMARIS Bitplane software for three-dimensional reconstruction and co-localization analysis. Laser and exposure settings are optimized to ensure consistency in signal detection and minimize variability. Approximately 6-8 lumbar V3 slices from L2- and L6 were imaged and analyzed for distinctions between long and short projection identities of V3V neurons per mouse (n = 3 mice), and a total of 18 slices across the 3 Mice.

3.6.3. Activity-Dependent Recruitment of V3 Neuron Subpopulations via cFos Expression-Objective 3

To evaluate the functional recruitment of V3V subpopulations, cFos expression was examined after segment-specific ventral root stimulation. Adult mice (both males (n=4) and

females (n=2); aged P56–P87) were used for this aim. Anesthesia was initially induced in a chamber using ~5% isoflurane in 95% oxygen until the righting reflex was lost. The Mice were then transferred to a mask to maintain an appropriate level of anesthesia (~2-2.5%) mixed with air. Each mouse was weighed for precise drug administration, and monitoring records were established.

Once under anesthesia, the mice were placed on a heated surgical pad to maintain normothermia, with a thermal probe placed on the pad for continuous temperature monitoring and feedback. An ophthalmic lubricant (Artificial Tears P.M.) was applied to prevent corneal dryness, which was followed by periodic visual assessment of respiration (breath per minute rate counts), mucosal colour, and reflexes. In addition, a pulse oximeter clip was attached to the forepaw to monitor heart rate, blood oxygen saturation and respiratory rate (PhysioSuite, Harward Apparatus). The surgical site was prepared by shaving the thoracolumbar region (T2–L6) as shown in Figure. 2B. A topical anesthetic (Lidocaine 2.5%) was administered at the incision sites approximately 15 minutes before the start of the surgical procedure to reduce pain stimuli resulting from cutting the skin.

Following pre-operative stabilization, the Mouse was positioned prone, and a midline incision was made to expose the dorsal thoracic to lumbar regions. Paraspinal muscles were dissected away to reveal the vertebrae (T1-L6), and hemostasis was maintained with sterile gauze and saline. A laminectomy was performed to access the lumbar spinal cord, and the dura was opened for visualization of the cord and nerve roots, which were kept moist with warm saline.

The dura mater was incised from caudal to rostral levels to provide clear visibility of the spinal cord and the emerging nerve roots. Using a surgical microscope, the L2 or L6 ventral roots

were located by gently separating the rootlets with fine glass rods and microdissection tools. The chosen ventral root was isolated while preserving its structural integrity.

A custom silver-silver chloride metal stimulating electrode was then positioned on the isolated ventral root. Functional verification of the electrode's placement and viability involved delivering brief test stimuli to elicit focal muscle contractions. For L2 stimulation, muscle contractions were predominantly observed in the proximal hindlimb musculature of the upper thigh region, while L6 stimulation elicited muscle contractions in more distal hindlimb muscles. These observations confirmed the accurate targeting of the ventral root. Before initiating sustained ventral root stimulation, the corresponding dorsal root was transected to eliminate sensory feedback and ensure that subsequent activations were confined to antidromic activation of motor axons. The stimulation threshold (TH) was established as the minimum intensity necessary to excite the most responsive axons through the ventral root. The stimulation intensity was then set to approximately 1.5x TH.

Continuous electrical stimulation was administered for 60–90 minutes using square pulses of 0.2 ms duration, arranged in trains of 9 pulses at 300 Hz, delivered at a 1 Hz train frequency. Stimulation lasted 90 minutes with amplitude parameters individualized for each mouse. During the stimulation period, the exposed spinal cord and nerve roots were covered with warm mineral oil to prevent desiccation and the preparation was kept under a radiant, infrared heat lamp with feedback. At the conclusion of the stimulation session, the stimulating electrode was removed from the ventral root, and the mouse remained under anesthesia for an additional 90-minute post-stimulation period to allow stabilization of activity-dependent gene expression and adequate protein synthesis for cFos detection. Control mice underwent identical surgical procedures, but no electrical stimulation was applied. After completing this experimental protocol, transcardial

perfusion of the mice was performed. The mouse was positioned supine, and a midline incision was made to access the thoracic cavity. A perfusion needle was inserted into the left ventricle, with an incision in the right atrium made for drainage of blood and perfusate.

Initial perfusion was 20-30 mL of 1x Phosphate-buffered saline (PBS) and heparin (0.1%) to remove blood from circulation. This was followed by 20-40 mL of 4% paraformaldehyde (diluted from 16% paraformaldehyde [PFA; Alfa Aesar] in PBS) for tissue fixation, followed by perfusion with 5 mL of 30% sucrose solution. Successful perfusion was indicated by a clear liver and extremities and the rigidity of the body. After fixation, the spinal cords were carefully dissected and post-fixed in PFA for 1 hour, then cryoprotected in 30% sucrose for immunohistochemical analysis. All remaining tissues were disposed of in accordance with institutional biohazard protocols.

Segment-Specific Analysis

The analysis primarily focused on segments directly involved in stimulation and on adjacent rostral segments. For L2 stimulation, the study examined both the L2 and L1 segments, while for L6 stimulation, the L6 and L5 segments were analyzed. This experimental design was intended to assess both local recruitment within the stimulated segments and intersegmental recruitment between adjacent areas.

To quantify cFos, V3 neurons were categorized by location and activity. They were classified as either $V3_{VM}$ $cFos^+$ neurons or $V3_{VL}$ $cFos^+$ neurons. The total counts of $V3_{VM}$ and $V3_{VL}$ neurons were determined, including the proportion of cFos-positive neurons within each subpopulation. This quantification enabled comparisons of recruitment patterns across various conditions, including the effects of rostral versus caudal stimulation, as well as differences between the $V3_{VM}$ and $V3_{VL}$ subpopulations. Additionally, the study assessed outcomes from stimulated

versus adjacent segments (specifically, L2 compared to L1 and L6 compared to L5) and contrasted results between stimulated and control Mice. Finally, due to differences in tissue recovery and segmental coverage between mice, the number of analyzed sections varied. Mouse 1 contained two analyzed sections within L6 and one section within L5, whereas Mouse 3 contained five analyzed sections within both L6 and L5, and six analyzed sections within the caudal S1 segment. Whereas Mice 2 and 4, containing 3 and 4 analyzed sections per segment, respectively.

Microscopy & Image Analysis

Sections were imaged using the Zeiss Axio Imager Z.2 at 10× for regional mapping and 40× magnification with Z-stack acquisition (~8–12 stacks) for precise identification of nuclear cFos immunoreactivity (TdTom double-labelled with cFos-A647^{+}). This was followed by importing the images into IMARIS Bitplane software for three-dimensional reconstruction and analysis. Laser settings were finely tuned and consistently applied across all slides to maintain imaging uniformity. Approximately 3-5 lumbar V3 slices sectioned from L2 and L1(for L2 stimulation) and L6 and L5 (for L6 stimulation) were imaged and analyzed to derive cFos activity of V3V neurons per mouse (n = 6 mice), with a total of 18 slices for the 6 Mice.

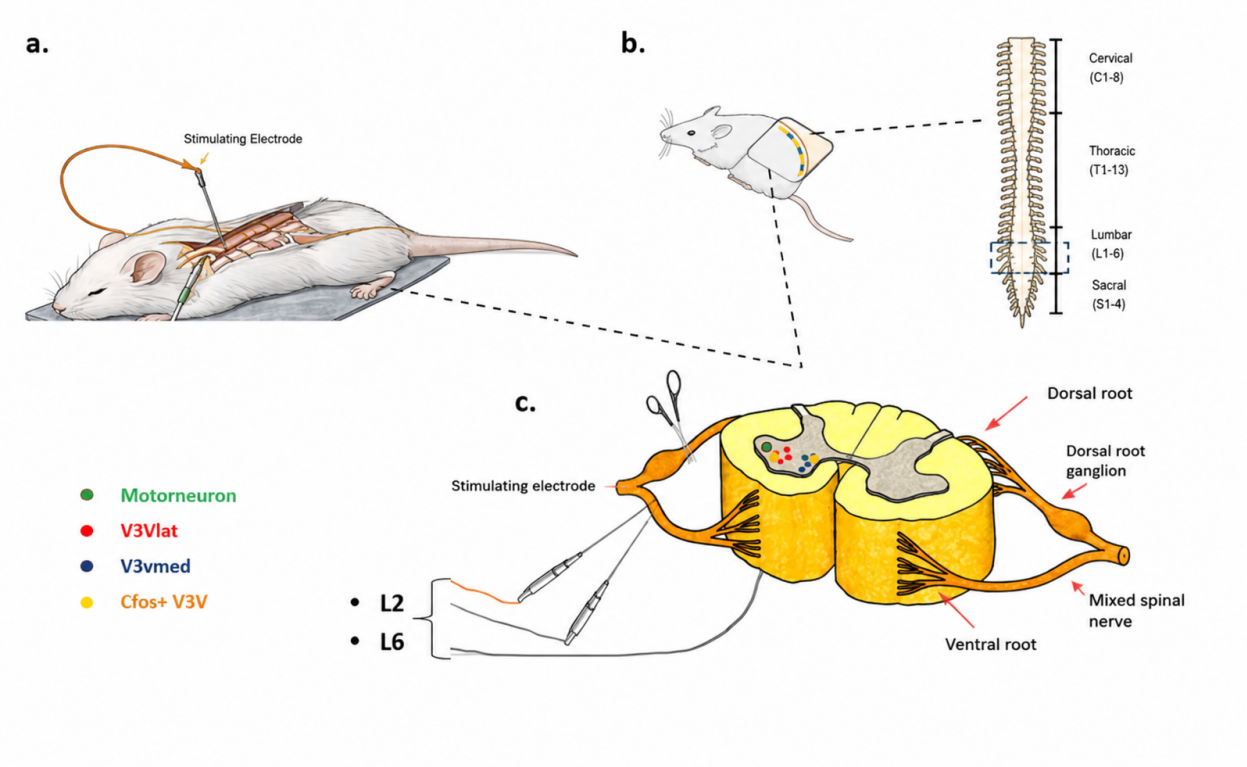

Figure 4: Summary of experimental procedure for evaluating the functional activation of V3 neuron subpopulations. A. Schematic illustration of where the laminectomy was applied for preparing the low-lumbar ventral roots for electrical stimulation. B. Depiction of the spinal cord's segmental organization, emphasizing the rostral (L2) and caudal (L6) lumbar levels targeted for 90 minutes of active stimulation and then 90 minutes without stimulation. C. Enlarged schematic of the intended ventral root activation, illustrating the medial ($V3_{VM}$) and lateral ($V3_{VL}$) subpopulations located within the ventral horn with a cut dorsal root at the same segmental level.

Chapter IV: Results

4.1 Segmental distribution of V3V subpopulations in adult lumbar spinal cord

Identification of Ventromedial and Ventrolateral V3 Subpopulations

Based on the classification from Chopek et al., we classified V3V neurons as medial ($V3_{VM}$) or lateral ($V3_{VL}$) based on their relative position within the ventral horn, using a mediolateral division defined as one-third of the ventral horn width measured from the midline, specific to each spinal segment. Neurons located within the medial third were categorized as $V3_{VM}$, whereas neurons located lateral to this boundary were categorized as $V3_{VL}$.

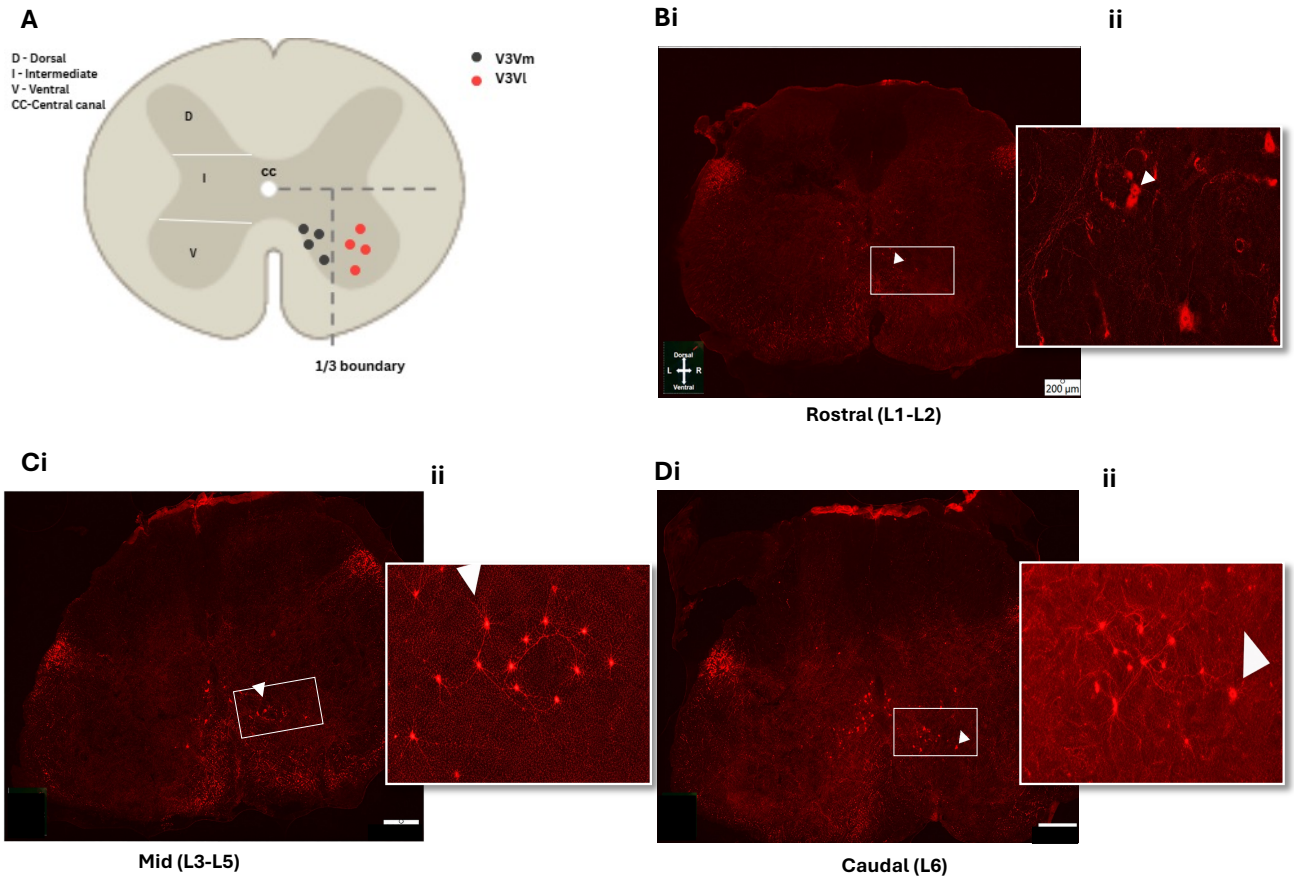

Figure 5: Anatomical identification of $V3_{VM}$ and $V3_{VL}$ subpopulations in the adult lumbar spinal cord. A) Schematic showing classification boundary outlining $V3_{VM}$ vs $V3_{VL}$ Bi) Rostral segment section (L1-L2 spinal cord) with inset highlighting the right V3Vs. ii) zoomed in inset in

Bi showing V3Vs with arrows c) Mid segment section (L3-L5) with inset highlighting the right V3Vs. ii) zoomed in inset in Ci showing V3Vs with arrows. d) Caudal segment section (L6) with inset highlighting the right V3Vs. ii) zoomed in inset in Di showing V3Vs with arrows. Scale bar 200um.

Rostrocaudal distribution of V3V subpopulations in individual Mice

To examine the segmental distribution of V3 neurons across the lumbar spinal cord, transverse sections spanning L1–L6 were sampled at inter-section intervals of approximately 264 μm, 320 μm and 349 μm, respectively, from 3 Mice. Sections were grouped into rostral (L1–L2), mid (L3–L5), and caudal (L6) regions to enable regional comparison.

Mouse 1

In mouse 1 (Figure 6), differences in the relative distribution of medial versus lateral V3V neurons were observed across the lumbar spinal cord. As shown in Figure 6e, of the 49 V3V neurons identified across 5 sections of the rostral lumbar segments (L1–L2), 42 (86%) were VM, and 7 (14%) were VL. In the mid-lumbar enlargement (L3–L5), the 79 V3V neurons identified across 7 sections were predominantly localized to the ventromedial domain, with only a small proportion occupying ventrolateral positions: 76 neurons (96%) VM; 3 neurons (4%) VL. In contrast, of the 46 V3V neurons across 3 sections, the caudal lumbar segment (L6) exhibited a marked increase in ventrolateral V3 representation: 32 neurons (70%) VM; 14 neurons (30%) VL, demonstrating a relatively greater representation of ventrolateral neurons than in the rostral and mid-lumbar segments. However, medial and lateral V3V neurons were both present in all segments.

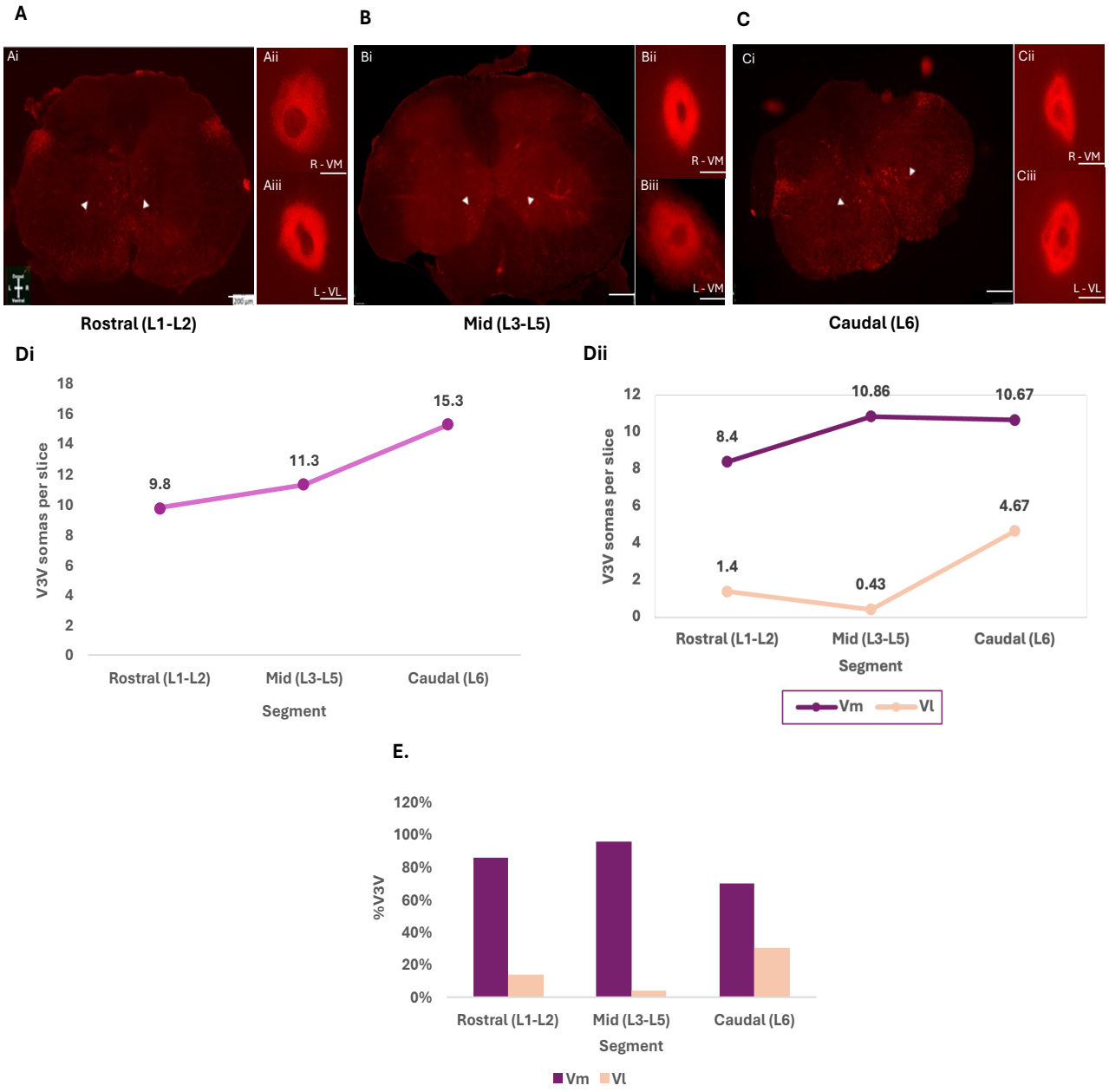

Figure 6: Segmental distribution of V3 subpopulations in Mouse 1. Ai). Representative transverse spinal cord sections from rostral (L1–L2) of V3Vs indicated by arrowhead (scale 200um), Aii-iii) inset demonstrating a right $V3_{VM}$ and left $V3_{VL}$ (10um). Bi.) mid (L3–L5), Bii-iii) with the right $V3_{VM}$ and the left $V3_{VM}$. Ci) and caudal (L6), Cii-iii) With the right $V3_{VM}$ and left $V3_{VM}$ lumbar segments showing V3 neuron labelling. Di.) Quantification of total V3V neurons across segments. Dii.) Distribution of $V3_{VM}$ and $V3_{VL}$ subpopulations across regions, E.) and proportion. Sections were sampled at ~264 µm intervals.

Mouse 2

In mouse 2 (Figure 7), a similar segmental pattern of V3V neuron distribution was observed. 66 V3V neurons were identified across 5 sections in the rostral lumbar segments (L1–L2), of which 54 (82%) were VM, and 12 (18%) were VL (Figure 7e). In the mid-lumbar segments (L3–L5), the 73 V3V neurons identified across 6 sections showed a strong predominance of ventromedial V3 neurons, with relatively low ventrolateral representation: 70 neurons (96%) VM; 3 neurons (4%) VL. This distribution shifted in the caudal segment (L6), where an increase in ventrolateral V3 neurons was evident. Of the 100 V3V neurons identified across 5 sections, 63 (63%) were VM, and 37 (37%) were VL. However, medial and lateral V3V neurons were present across all segments. Overall, the spatial organization closely mirrored that observed in Mouse 1 (Figure 6).

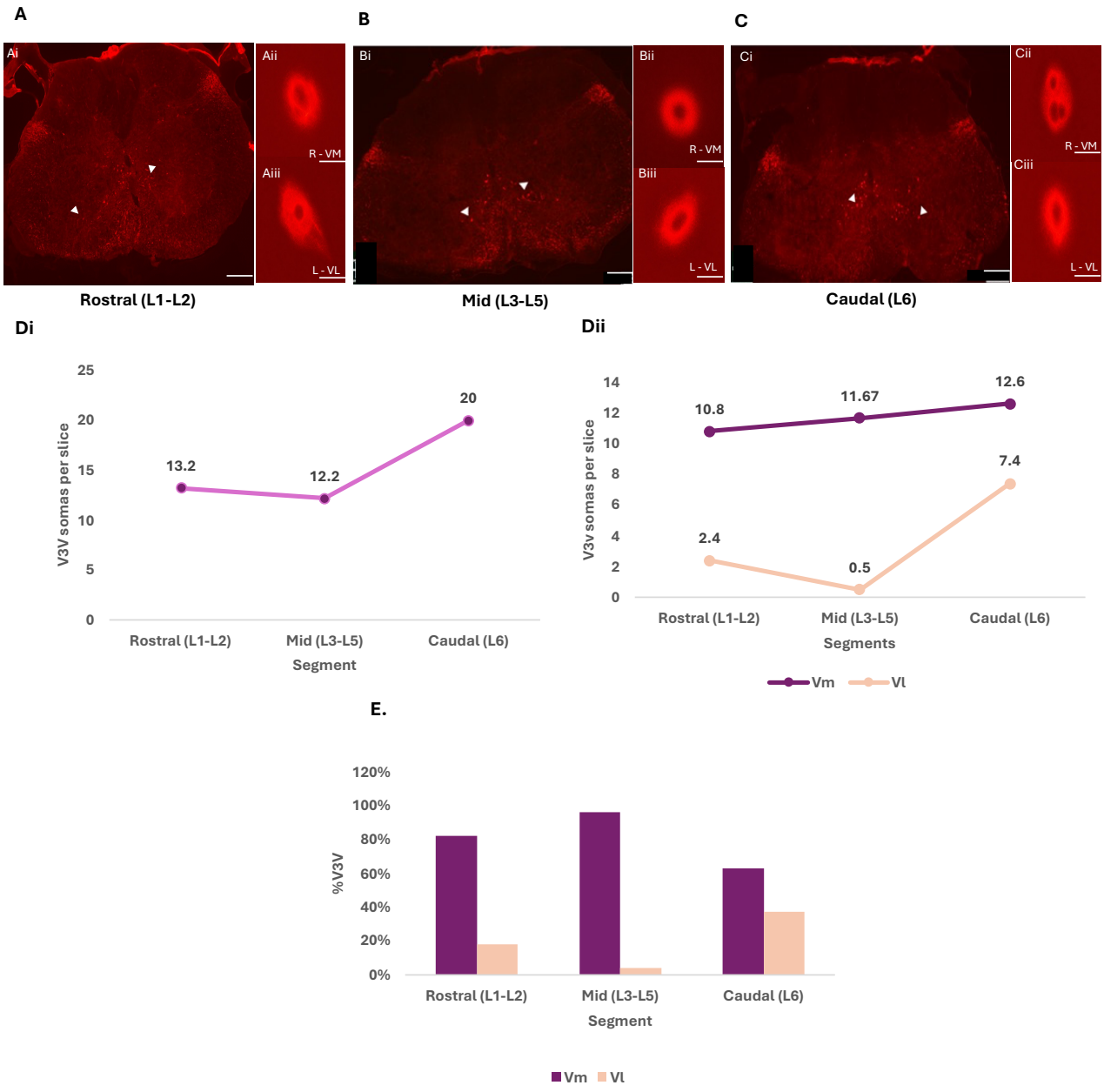

Figure 7: Segmental distribution of V3 subpopulations in Mouse 2. Ai). Representative transverse spinal cord sections from rostral (L1–L2) of V3Vs indicated by arrowhead (scale 200um), Aii-iii) with right $V3_{VM}$ and left $V3_{VL}$ (10um). Bi.) mid (L3–L5), Bii-iii) inset demonstrating a right $V3_{VM}$ and left $V3_{VL}$. Ci) and caudal (L6), Cii-iii) With the right $V3_{VM}$ and left $V3_{VM}$ lumbar segments showing V3 neuron labelling. Di.) Quantification of total V3V neurons across segments. Dii.) Distribution of $V3_{VM}$ and $V3_{VL}$ subpopulations across regions, E.) and proportion. Sections were sampled at ~320 µm intervals

Mouse 3

In mouse 3 (Figure 8), the segment-dependent distribution of V3V neurons was consistent with the patterns observed in the other mice. Figure 8 shows that of the 82 V3V neurons identified across 8 sections in the rostral lumbar segments (L1–L2), 58 (71%) were VM and 24 (29%) were VL. In the mid-lumbar region (L3–L5), the 86 V3V neurons identified across 10 sections were largely restricted to the ventromedial domain, with minimal ventrolateral representation: 73 neurons (85%) VM; 13 neurons (15%) VL. However, in the caudal segment (L6), of the 98 V3V neurons identified across 6 sections, there was a pronounced increase in ventrolateral V3 neurons, bringing the distribution to an intermediate ratio: 54 neurons (55%) VM; 44 neurons (45%) VL, reflecting a relatively greater representation of ventrolateral neurons than in the rostral and mid-lumbar segments Overall, the spatial organization and pattern closely mirrored that observed in mice 1 & 2. It is worth noting that, due to differences in sectioning thickness (20um versus 30um in the other 2 mice), the specific numbers were slightly higher than those of the other mice, as the pattern shift was observed late in the segmental gradient.

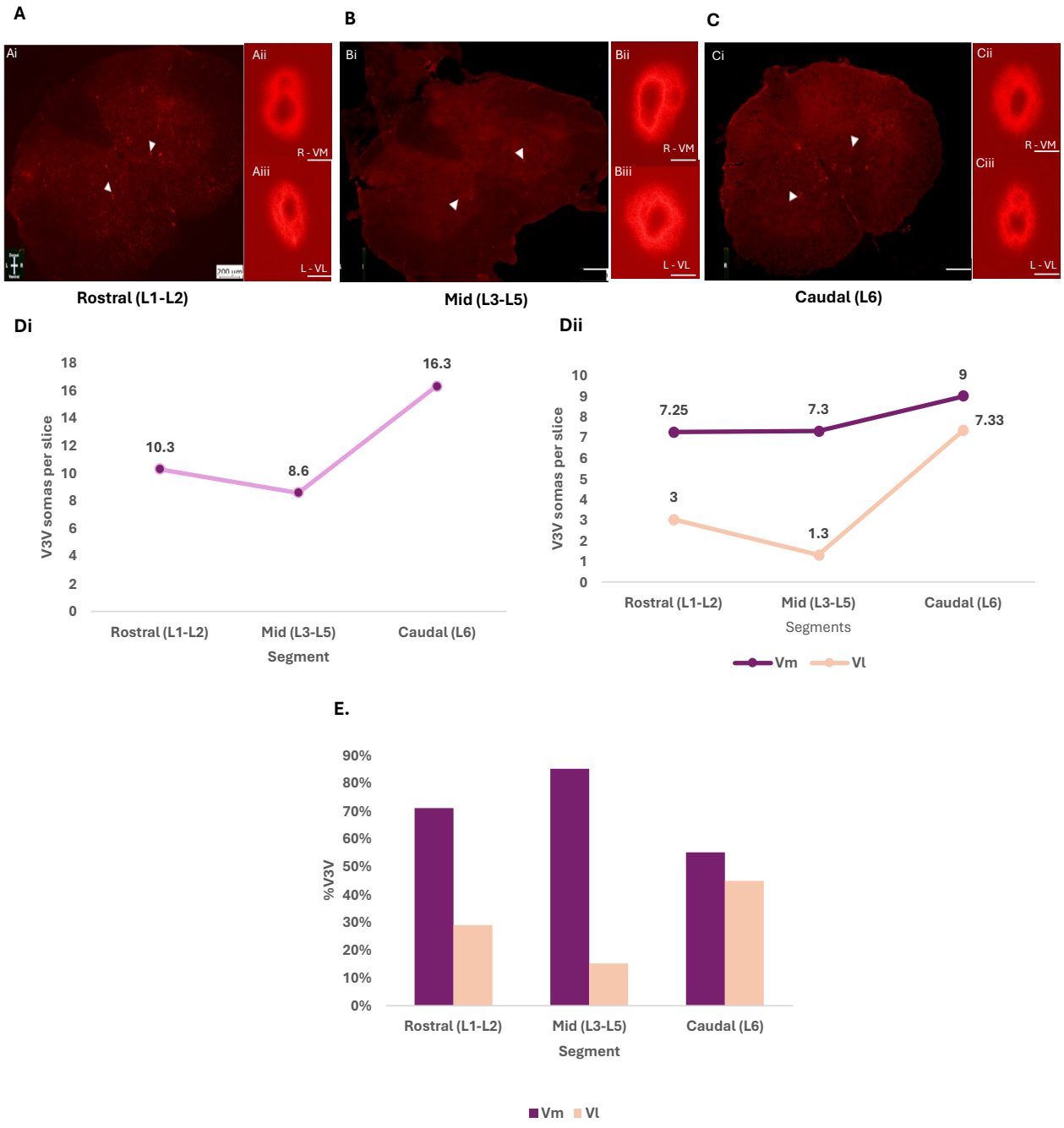

Figure 8: Segmental distribution of V3 subpopulations in Mouse 3. Ai). Representative transverse spinal cord sections from rostral (L1–L2) of V3Vs indicated by arrowhead (scale 200um), Aii-iii) with right $V3_{VM}$ and left $V3_{VL}$ (10um). Bi.) mid (L3–L5), Bii-iii) Inset demonstrating a right $V3_{VM}$ and left $V3_{VL}$. Ci) and caudal (L6), Cii-iii) With the right $V3_{VM}$ and left $V3_{VM}$ lumbar segments showing V3 neuron labelling. Di) Quantification of total V3V neurons across segments. Dii) Distribution of $V3_{VM}$ and $V3_{VL}$ subpopulations across regions, E.) and proportion. Sections were sampled at ~349 µm intervals.

Consistent segmental distribution patterns of V3 subpopulations across Mice

Cross-Mouse comparison

Across all three mice (Figure 9), a consistent segment-dependent difference in medial versus lateral representation of V3V neurons was observed along the rostrocaudal axis. In the rostral lumbar segments (L1–L2), of the total V3V neurons identified, VM neurons represented 71-86%, and VL represented 14-29%. In the mid-lumbar enlargement (L3–L5), 85-96% of the V3V neurons identified were predominantly ventromedial with minimal ventrolateral V3 neurons (4-15%), while the caudal lumbar segment (L6) exhibited an increase in ventrolateral representation (55-90% VM; 30-45% VL) of the total V3V neurons. These values are presented descriptively because of the limited sample size (n = 3 animals). While minor variations in spatial distribution and clustering were observed among mice, the overall pattern of increased ventrolateral representation in mid-to-caudal segments was conserved. These findings suggest a reproducible organizational pattern of V3 neurons within the lumbar spinal cord. This rostrocaudal variation may reflect segment-specific roles of V3 neurons in the organization of locomotor circuits and motor output control.

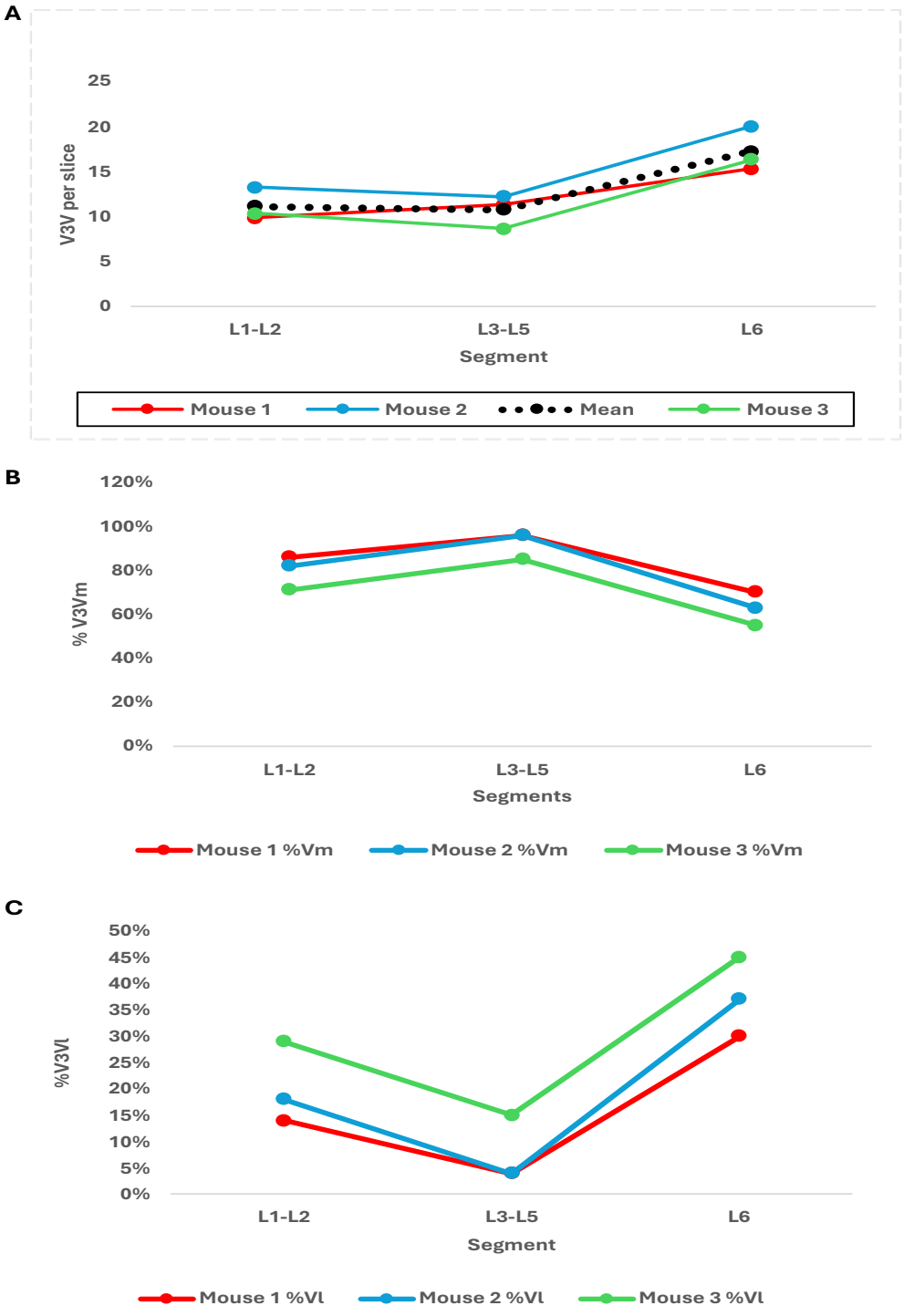

Figure 9: Comparison of rostrocaudal distribution and V3 subpopulation composition across Mice. a.) Comparison of total V3V neurons across rostral (L1–L2), mid (L3–L5), and caudal (L6) lumbar segments for Mice 1–3. b.) Comparison of $V3_{VM}$ proportional representation (%) across rostrocaudal regions for Mice 1–3. c.) Comparison of $V3_{VL}$ proportional representation (%) across

rostrocaudal regions for Mice 1–3. Sections were sampled at ~264 µm, 320 µm and 349 µm intervals, respectively, across L1–L6. Data are presented for three Mice.

4.2 Characterization of Projection Patterns of V3V Neurons Using Zfhx3 and NFIB Molecular Markers

To begin characterizing projection-associated molecular identities within V3V neurons, expression of Zfhx3 and NFIB was examined in the rostral (L2) and caudal (L6) lumbar segments in two mice. Both markers were detected within subsets of $V3_{VM}$ and $V3_{VL}$ neurons (Figures 10 & 11). Figures 10A, B, and 11A, B show immunofluorescence images illustrating Zfhx3 and NFIB expression in L2 and L6 tdTomato-positive V3V neurons, respectively. These images are presented to demonstrate marker expression and localization and are not intended to represent the quantitative data. Quantitative analyses were performed across all analyzed sections from each animal. For Zfhx3, four L2 and four L6 sections were analyzed in mouse 1, while two L2 and three L6 sections were analyzed in mouse 2. In mouse 1 (Figure 10C), 5 of 7 identified $V3_{VM}$ neurons (71%) and 1 of 1 identified $V3_{VL}$ neurons (100%) at L2 were Zfhx3-positive. At L6, 14 of 16 identified $V3_{VM}$ neurons (88%) and 4 of 4 identified $V3_{VL}$ neurons (100%) expressed Zfhx3. In mouse 2 (Figure 10C), 12 of 20 identified $V3_{VM}$ neurons (60%) and 5 of 7 identified $V3_{VL}$ neurons (71%) at L2 were Zfhx3-positive. At L6, 12 of 29 identified $V3_{VM}$ neurons (41%), and 16 of 20 identified $V3_{VL}$ neurons (80%) expressed Zfhx3. Combined, this was an average of 65.5% $V3_{VM}$ neurons and 85.5% $V3_{VL}$ neurons that were L2 Zfhx3-positive, and 64.5% $V3_{VM}$ neurons and 90% $V3_{VL}$ neurons that were Zfhx3-positive. Zfhx3 expression was therefore observed in V3V subpopulations but appeared more prevalent among $V3_{VL}$ neurons, particularly in the caudal lumbar cord. For NFIB, six L2 and six L6 sections were analyzed in mouse 1, while two L2 and three L6 sections were analyzed in mouse 2. In mouse 1 (Figure 11C), 10 of 16 identified $V3_{VM}$ neurons (63%) and 2 of 5 identified $V3_{VL}$ neurons (40%) at L2 were NFIB-positive. At L6, 26 of

40 identified $V3_{VM}$ neurons (65%) and 8 of 8 identified $V3_{VL}$ neurons (100%) expressed NFIB. In mouse 2 (Figure 11C), 10 of 14 identified $V3_{VM}$ neurons (71%) and 7 of 11 identified $V3_{VL}$ neurons (64%) at L2 were NFIB-positive. At L6, 13 of 24 identified $V3_{VM}$ neurons (54%) and 3 of 10 identified $V3_{VL}$ neurons (30%) expressed NFIB. Combined, this was an average of 67% $V3_{VM}$ neurons and 52% $V3_{VL}$ neurons that were L2 NFIB-positive, and 59.5% $V3_{VM}$ neurons and 65% $V3_{VL}$ neurons that were NFIB-positive. In contrast to Zfhx3, NFIB expression was observed at comparable proportions across $V3_{VM}$ and $V3_{VL}$ populations. These preliminary observations suggests that V3V neurons may comprise of molecularly heterogeneous populations expressing transcription factors associated with putative long- and short-range projection identities. It is noted that the percentage is relative to each antibody examined, as we did not examine both antibodies in individual sections or in serial sections to determine the exclusivity of expression between the two populations. This is noted in the limitation section in the discussion.

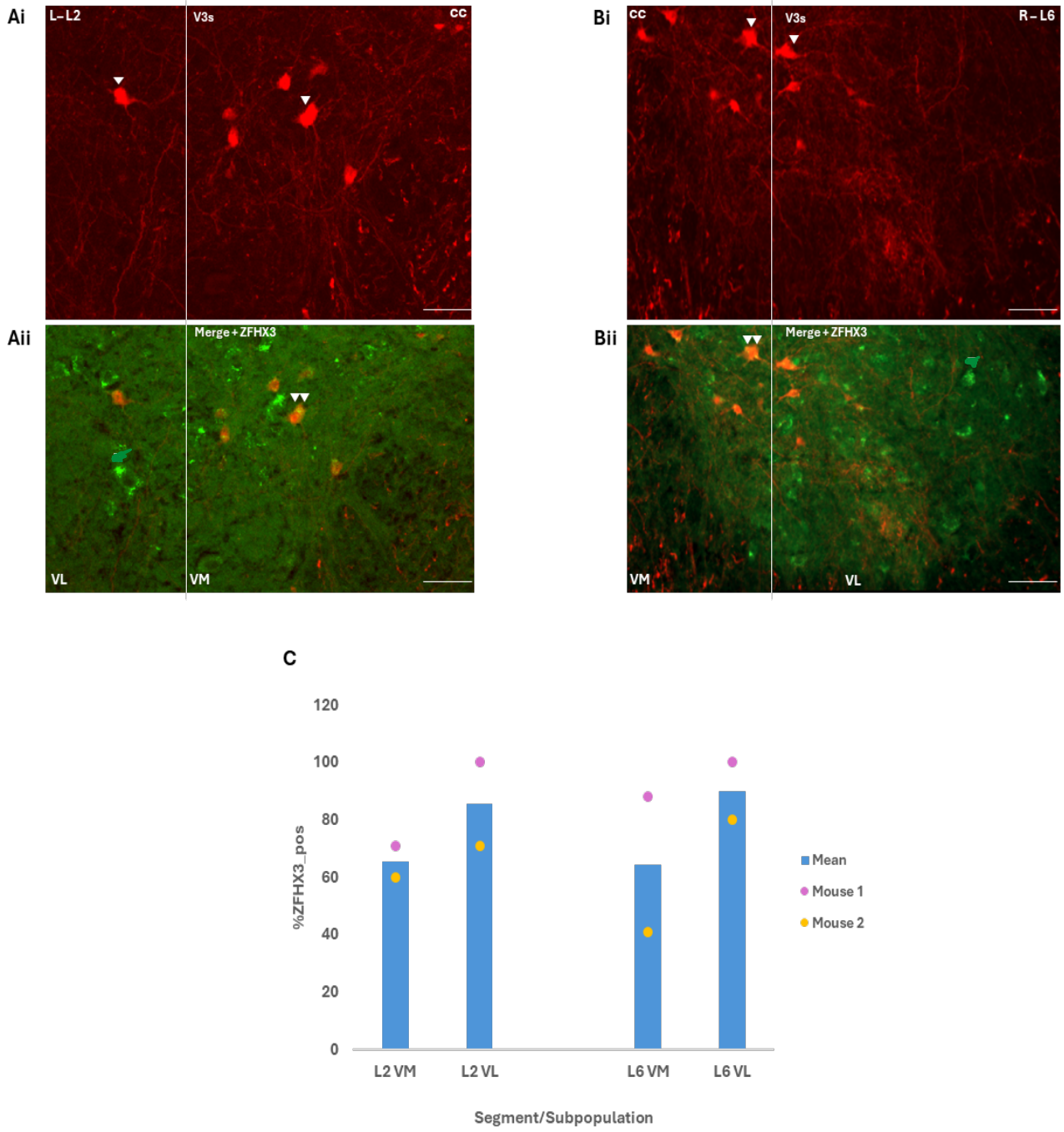

Figure 10: Molecular characterization of V3V neuron subpopulations using projection-associated transcription factor Zfhx3.
Ai). Immunoflourescence images from lumbar L2 spinal cord sections, and Bi) lumbar L6 spinal cord sections showing tdTomato-labelled V3V neurons (red) and ii) Zfhx3 immunoreactivity (green). Single arrowheads indicate V3 neurons, while double arrowheads indicate Zfhx3-positive V3 neurons. VL and VM ventral horn regions are shown. Scale bars = 50 µm. C) Quantification of Zfhx3-positive $V3_{VM}$ and $V3_{VL}$ neurons within L2 and L6 segments in mouse 1 & 2. Data are presented as the proportion (%) of Zfhx3-positive neurons (y-axis), mean of the two mice (bars),

and % Zfhx3+ of mice 1 & 2 (dots) within each V3V subpopulation. Quantification was performed from four L2 and four L6 sections in mouse 1 and two L2 and three L6 sections in mouse 2. Therefore, the values shown in C are not derived only from the images in panels A and B.

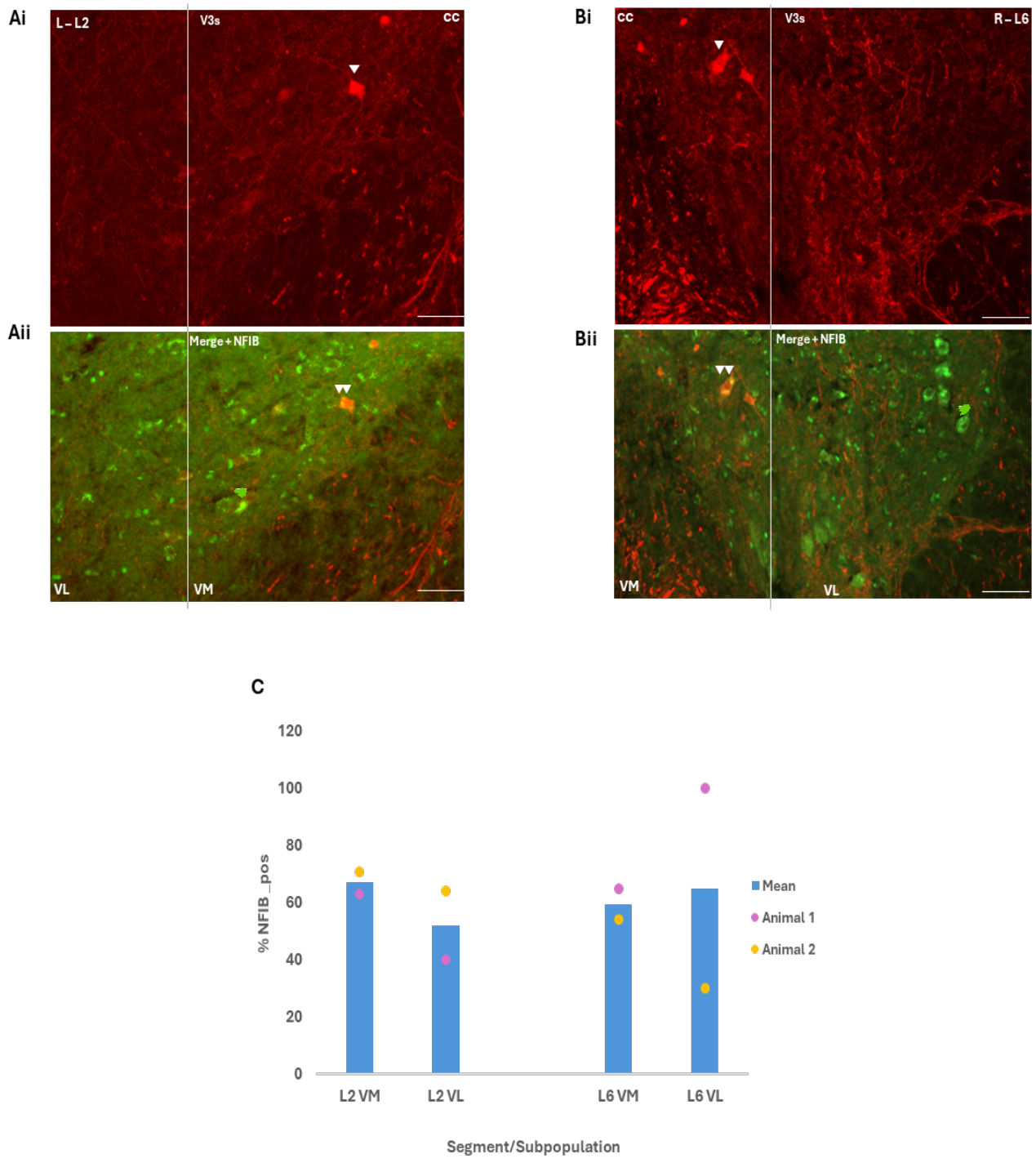

Figure 11: Molecular characterization of V3V neuron subpopulations using projection-associated transcription factor NFIB.

Ai). Immunofluorescence images from lumbar L2 spinal cord sections, and Bi) lumbar L6 spinal cord sections showing tdTomato-labelled V3V neurons (red) and ii) NFIB immunoreactivity (green). Single arrowheads indicate V3 neurons, while double arrowheads indicate NFIB-positive V3 neurons. VL and VM ventral horn regions are shown. Scale bars = 50 μm. C) Quantification of NFIB-positive $V3_{VM}$ and $V3_{VL}$ neurons within L2 and L6 segments in mouse 1 & 2. Data are presented as the proportion (%) of NFIB-positive neurons (y-axis), mean of the two mice (bars), and % NFIB+ of mice 1 & 2 (dots) within each V3V subpopulation. Quantification was performed from six L2 and six L6 sections in mouse 1 and two L2 and three L6 sections in mouse 2. Therefore, the values shown in C are not derived only from the images in panels A and B.

4.3 Activity-dependent recruitment of $V3_{VM}$ and $V3_{VL}$ neurons after L2 or L6 ventral root stimulation

To evaluate the recruitment of V3V subpopulations by activation of segment-specific motor pathways, we measured cFos expression in $V3_{VM}$ and $V3_{VL}$ neurons in response to stimulation of the L2 or L6 ventral roots. In response to VR stimulation, cFos expression was assessed in both the segment above and below the stimulated ventral root. Within each segment, V3 neurons were categorized as either ventromedial or ventrolateral, and we calculated the proportions of cFos-positive and cFos-negative V3 neurons.

L2 stimulation produced broad recruitment of $V3_{VM}$ and $V3_{VL}$ neurons in L2 and L1

In response to stimulation of the L2 ventral root, cFos expression was examined in the L1 and L2 lumbar spinal cord segments. Figure 12A shows immunofluorescence images illustrating cFos expression in tdTomato-positive V3V neurons following L2 ventral root stimulation. These images are presented to demonstrate cFos immunoreactivity and localization and are not intended to represent the quantitative data. Quantitative analyses were performed across all analyzed sections from each animal. Three sections each from the L1 and L2 segments were analyzed in mouse 2, while four sections each from the L1 and L2 segments were analyzed in mouse 4. cFos expression was detected in both $V3_{VM}$ and $V3_{VL}$ populations within the L1 and L2 spinal segments (Figure 12). In mouse 2, the identified L2 neurons were 42 $V3_{VM}$ neurons and 11 $V3_{VL}$ neurons. Of these,

21 $V3_{VM}$ neurons (50%) and 7 $V3_{VL}$ neurons (64%) were cFos-positive (Figure 12a, b). In the L1 segment, 32 $V3_{VM}$ and 15 $V3_{VL}$ neurons were identified, with 13 $V3_{VM}$ neurons (41%) and 4 $V3_{VL}$ neurons (27%) expressing cFos. Similarly, in mouse 4, the numbers of the identified L2 neurons were 37 $V3_{VM}$ and 17 $V3_{VL}$, of which 20 $V3_{VM}$ (54%) and 8 $V3_{VL}$ (47%) were cFos-positive. Within the L1 segment, 39 $V3_{VM}$ neurons and 20 $V3_{VL}$ neurons were identified, with cFos expression detected in 24 $V3_{VM}$ neurons (62%) and 13 $V3_{VL}$ neurons (65%).

Overall, the proportion of cFos-positive $V3_{VM}$ neurons in the stimulated L2 segment ranged from 50–54%, while $V3_{VL}$ activation ranged from 47–64% (Figure 12a, b). In the L1 segment, cFos expression was observed in both populations, although the relative recruitment patterns varied across mice (41–62% VM; 27–65% VL). These preliminary findings suggest that L2 ventral root stimulation recruits both medial and lateral V3V subpopulations within the stimulated segment and may additionally engage V3V neurons in adjacent rostral lumbar circuits.

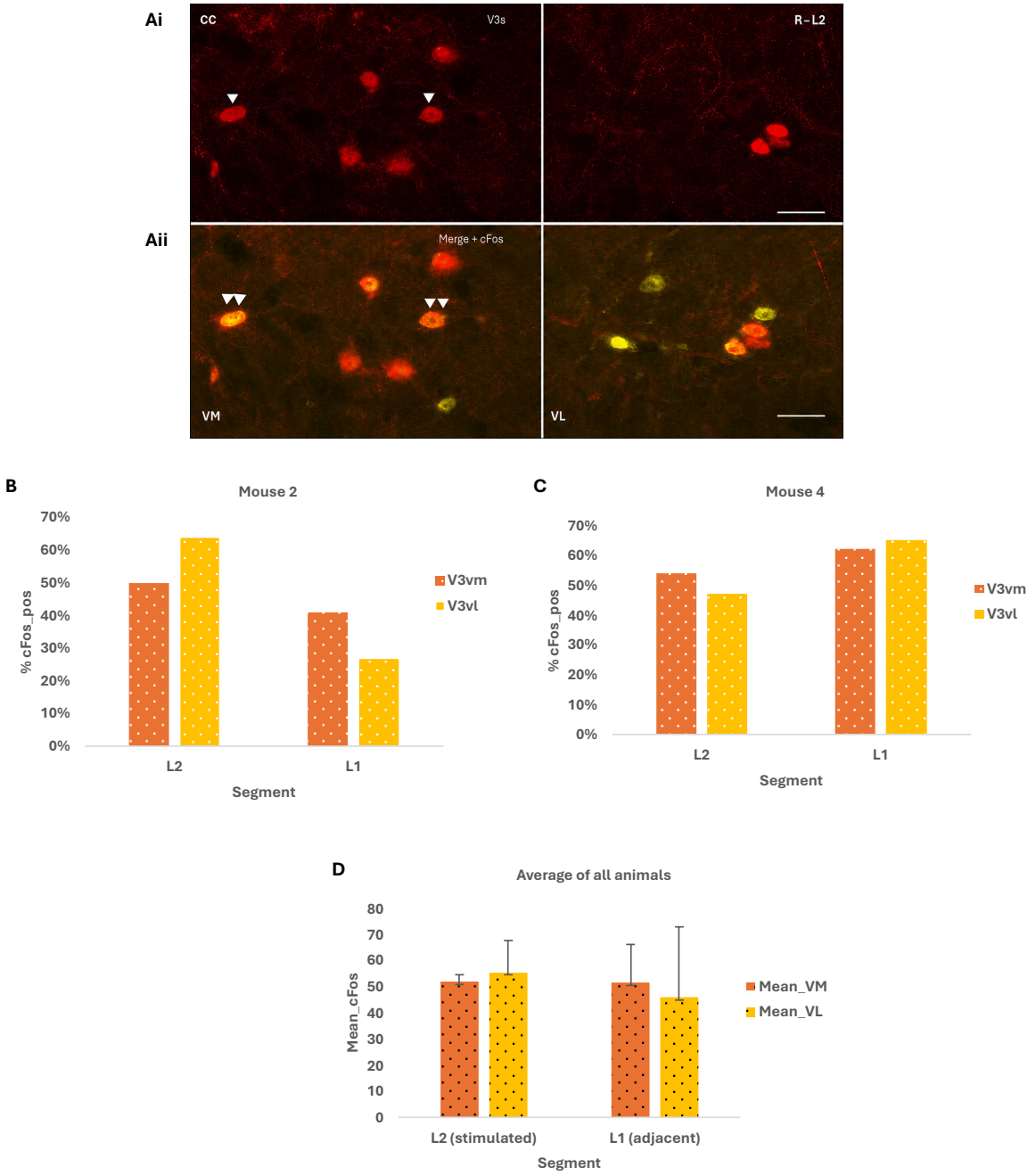

Figure 12: Segment-specific cFos activation of V3V neurons following L2 stimulation. (A) Immunofluorescence images from lumbar L2 spinal cord sections showing tdTomato-labelled V3V neurons (red) and cFos immunoreactivity (yellow). Single arrowheads indicate V3 neurons, while double arrowheads indicate cFos-positive V3 neurons. VL and VM ventral horn regions are shown. Scale bars = 50 µm. (B-C) Representative quantification of cFos-positive $V3_{VM}$ and $V3_{VL}$ neurons in individual Mice following L2 stimulation, comparing the stimulated segment (L2) and adjacent segment (L1). (D) Grouped data showing the mean percentage of cFos-positive $V3_{VM}$ and $V3_{VL}$ neurons across Mice. Error bars represent standard deviation. Quantification was performed from three L2 and three L1 sections in mouse 2 and four L2 and four L1 sections in mouse 4. Therefore, the values shown in B, C, and D, are not derived only from the image in panel A.

L6 stimulation showed variable but strong recruitment of caudal V3 subpopulations

In response to L6 ventral root stimulation, cFos expression was examined in the L5, L6, and caudal S1 spinal cord segments. Figure 13A, 14A and 14B show immunofluorescence images illustrating cFos expression in tdTomato-positive V3V neurons following L6 ventral root stimulation. These images are presented to demonstrate cFos immunoreactivity and localization and are not intended to represent the quantitative data. Quantitative analyses were performed across all analyzed sections from each animal. In mouse 1, two L6 sections and one L5 section were analyzed. In mouse 3, five sections each from the L6 and L5 segments and six sections from the caudal S1 segment were analyzed. cFos expression was detected in both $V3_{VM}$ and $V3_{VL}$ populations across the analyzed spinal segments (Figures 13 and 14). In mouse 1, 8 $V3_{VM}$ neurons and 15 $V3_{VL}$ neurons were identified in the L6 segment. Of these, 6 $V3_{VM}$ neurons (75%) and 4 $V3_{VL}$ neurons (27%) were cFos-positive (Figure 13a, b). In the L5 segment, 5 $V3_{VM}$ neurons and 4 $V3_{VL}$ neurons were identified, with no detectable cFos expression observed in either population (0% VM; 0% VL). In Mouse 3, the identified L6 neurons showed a larger V3V population, including 51 $V3_{VM}$ and 40 $V3_{VL}$ neurons. Of these, 37 $V3_{VM}$ (73%) and 24 $V3_{VL}$ (60%) neurons were cFos-positive. Within the L5 segment, 66 $V3_{VM}$ neurons and 46 $V3_{VL}$ neurons were identified, with cFos expression detected in 32 $V3_{VM}$ neurons (48%) and 42 $V3_{VL}$ neurons (91%). Additional analysis of the caudal S1 segment in Mouse 3 demonstrated persistent recruitment beyond the stimulated lumbar segment. Across six analyzed S1 sections, 47 $V3_{VM}$ neurons and 48 $V3_{VL}$ neurons were identified, with cFos expression observed in 38 $V3_{VM}$ neurons (81%) and 28 $V3_{VL}$ neurons (58%) (Figure 14c).

Overall, $V3_{VM}$ neurons within the stimulated L6 segment consistently exhibited high levels of cFos activation across mice (73–75%) (Figure 13a, b). In contrast, $V3_{VL}$ recruitment within L6 was more variable (27–60%). Recruitment patterns within the L5 segment also differed markedly among mice, ranging from no activation in mouse 1 to greater recruitment in mouse 3, particularly in the $V3_{VL}$ population (91% VL). Together, these preliminary findings suggest that L6 ventral root stimulation more strongly recruits caudal V3V populations, while the spread of activation to adjacent and more caudal segments exhibits considerable inter-mouse variability.

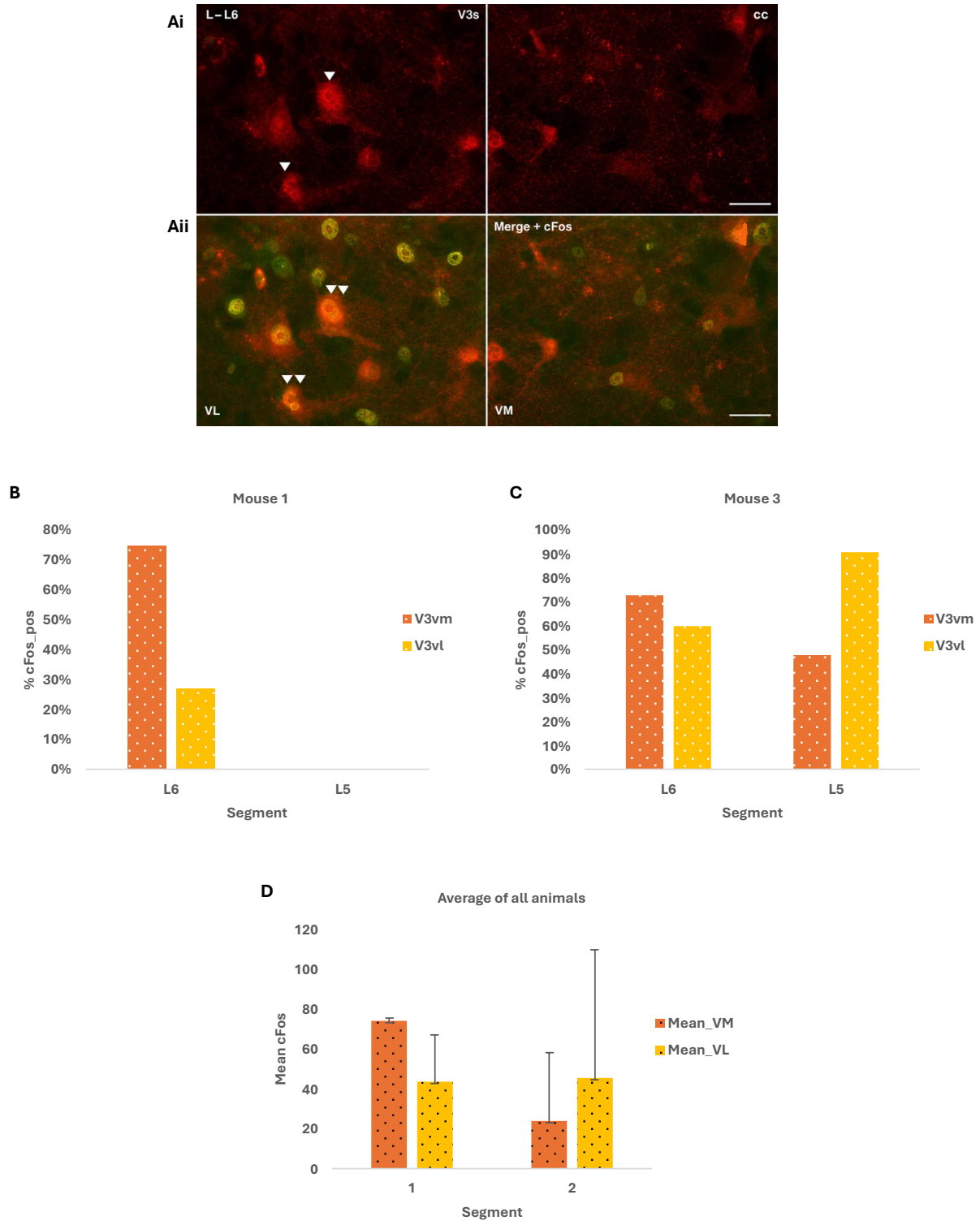

Figure 13: Segment-specific cFos activation of V3V neurons following L6 stimulation. (A) Immunofluorescence images from lumbar L6 spinal cord sections showing tdTomato-labelled V3*V* neurons (red) and cFos immunoreactivity (yellow). Single arrowheads indicate V3 neurons, while double arrowheads indicate cFos-positive V3 neurons. VL and VM ventral horn regions are shown. Scale bars = 50 µm. (B-C) Representative quantification of cFos-positive $V3_{VM}$ and $V3_{VL}$

neurons in individual Mice following L6 stimulation, comparing the stimulated segment (L6) and adjacent segment (L5). (D) Grouped data showing the mean percentage of cFos-positive $V3_{VM}$ and $V3_{VL}$ neurons across Mice. Error bars represent standard deviation. Scale bar = 50 µm. Quantification was performed from two L6 and one L1 sections in mouse 1 and five L2 and five L1 sections in mouse 3. Therefore, the values shown in B, C, and D, are not derived only from the image in panel A.

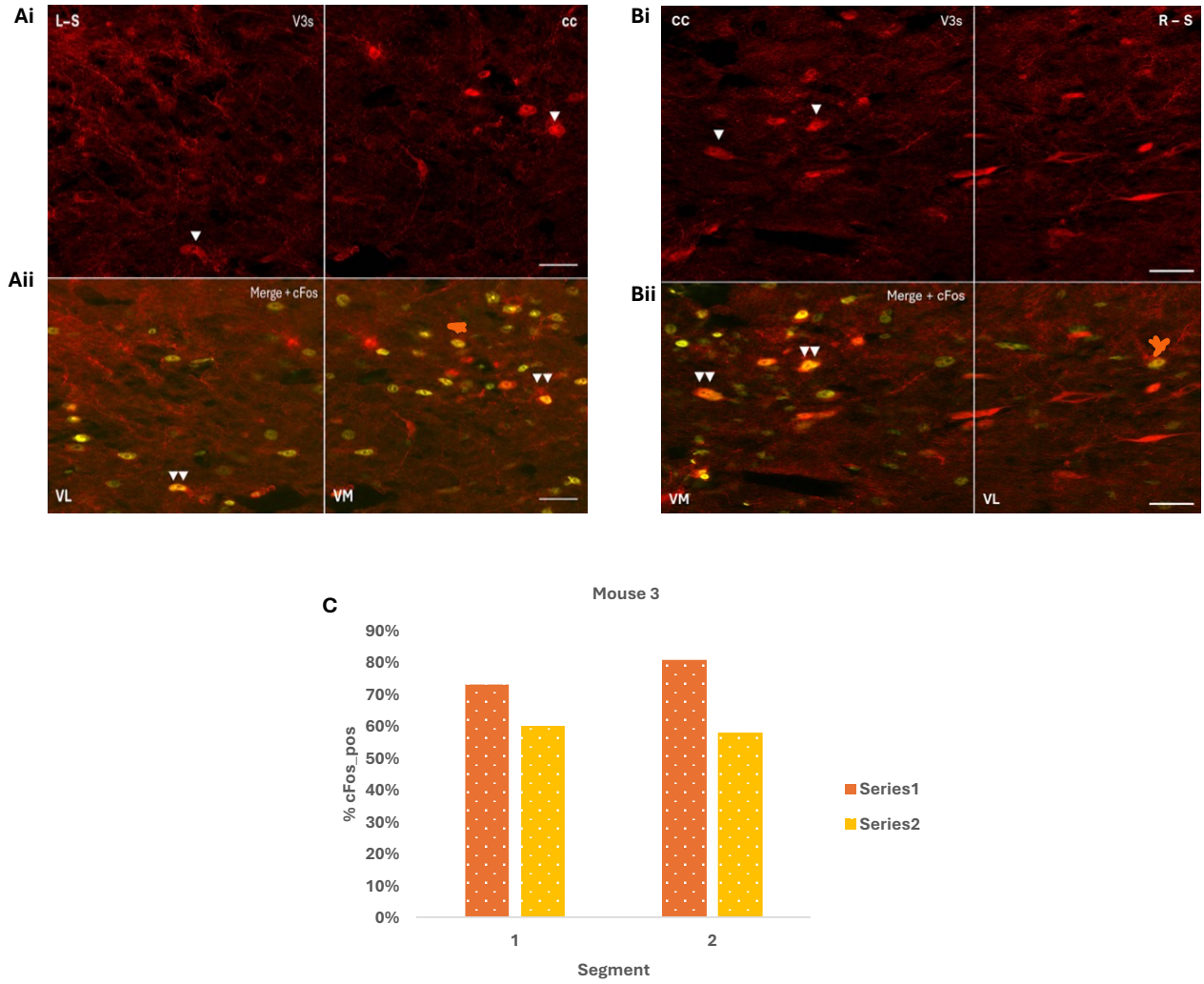

Figure 14: cFos recruitment within V3V subpopulations in the caudal S1 segment following L6 ventral root stimulation.
(Ai–Bi) Immunofluorescence images showing tdTomato+ V3V neurons (red) and cFos immunoreactivity (yellow) within the S1 segment of an L6-stimulated animal (mouse 3). Left and right hemicords are shown separately, with VM and VL regions indicated. Single arrowheads identify representative V3 neurons. (Aii–Bii) Merged images illustrating co-localization of cFos

within $V3_{VM}$ and $V3_{VL}$ populations in the S1 segment. (C) Quantification of cFos-positive neurons within V3V subpopulations in S1, demonstrating recruitment of both $V3_{VM}$ (81%) and $V3_{VL}$ (58%) neurons following L6 ventral root stimulation. Data are presented as the percentage of cFos-positive neurons within each V3 subpopulation. Scale bars = 50 µm. Quantification was performed from six S1 sections in mouse 3. Therefore, the values shown in C are not derived only from the images in panels A and B.

Non-stimulated control animal exhibited low-to-moderate baseline cFos expression across V3V subpopulations.

To assess baseline neuronal activity in the absence of ventral root stimulation, cFos labelling was quantified in a non-stimulated control mouse (mouse 5; male) across the L2 and L1 lumbar segments (Figure 15). Figure 15A shows immunofluorescence images illustrating cFos expression in tdTomato-positive V3V neurons in the absence of ventral root stimulation. These images are presented to demonstrate cFos immunoreactivity and localization and are not intended to represent the quantitative data. Four sections were analyzed per segment using the same systematic sampling approach applied to stimulated mice. Within the L2 segment, a total of 26 $V3_{VM}$ neurons and 9 $V3_{VL}$ neurons were identified. Of these, 9 $V3_{VM}$ neurons (35%) and 4 $V3_{VL}$ neurons (44%) were cFos-positive, while the remaining V3 neurons were cFos-negative (65% VM; 56% VL). In the adjacent L1 segment, 19 $V3_{VM}$ neurons and 11 $V3_{VL}$ neurons were identified, with cFos expression observed in 10 $V3_{VM}$ neurons (53%) and 4 $V3_{VL}$ neurons (36%).

Overall, of the 65 V3V neurons identified across 8 sections, 27 expressed cFos, suggesting that the non-stimulated control mouse showed detectable baseline cFos expression in both the medial and lateral V3V populations. Similar to the stimulated mice, cFos-positive neurons were observed in both the L2 and adjacent L1 segments. However, following L2 ventral root stimulation, the proportion of cFos-positive $V3_{VM}$ neurons within the L2 segment ranged from 50-

54%, compared with 35% in the non-stimulated control, while $V3_{VL}$ activation ranged from 47-64% compared with 44% in the control. In the adjacent L1 segment, cFos expression was also detected in both $V3_{VM}$ and $V3_{VL}$ populations in stimulated and control animals, although the relative proportions varied among mice. These preliminary findings suggest basal neuronal activity in V3V neurons under resting conditions and provide an important reference for interpreting activity-dependent recruitment following stimulation of the L2 and L6 ventral roots.

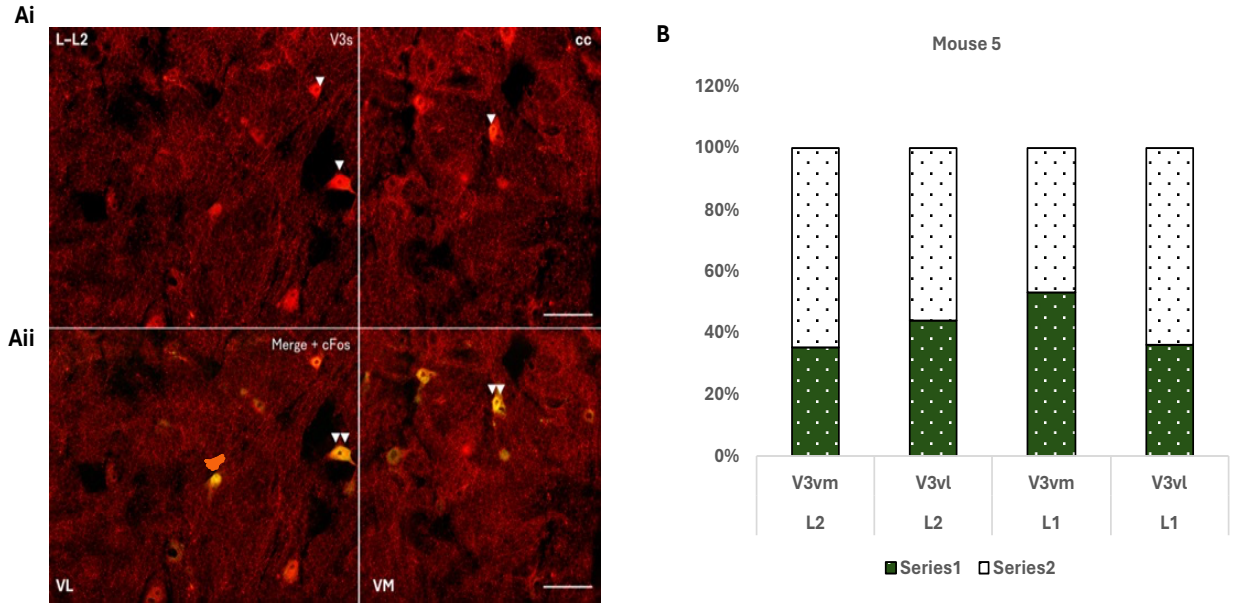

Figure 15: Baseline cFos expression in V3V subpopulations of a non-stimulated control animal.
(A) Immunofluorescence images from lumbar L1–L2 spinal cord sections showing tdTomato-labelled V3V neurons (red) and cFos immunoreactivity (yellow). Single arrowheads indicate V3 neurons, while double arrowheads indicate cFos-positive V3 neurons. VL and VM ventral horn regions are shown. Scale bars = 50 µm. (B) Quantification of cFos-positive and cFos-negative $V3_{VM}$ and $V3_{VL}$ neurons within L2 and adjacent L1 segments in the non-stimulated control animal (Mouse 5). Data are presented as the proportion (%) of cFos-positive and cFos-negative neurons within each V3*V* subpopulation. Baseline cFos expression was detected in both medial and lateral V3 populations in the absence of ventral root stimulation. Quantification was performed from four L2 and four L1 sections in mouse 5. Therefore, the values shown in B are not derived only from the image in panel A.

<u>Comparison of L2 and L6 stimulation patterns</u>

Comparative analysis of ventral root stimulation at L2 and L6 across the stimulated animals revealed distinct patterns of neural recruitment among V3V subpopulations (Figure 16). Stimulation at the L2 level in the n=2 mice examined suggests a relatively uniform activation of both $V3_{VM}$ and $V3_{VL}$ neurons in the L2 and L1 segments (L2: 50–54% VM; 47–64% VL) (Figure. 16b), corresponding to mean activation levels of approximately 52% for $V3_{VM}$ and 55.5% for $V3_{VL}$ in L2 (Figure. 16a). In the adjacent L1 segment, activation remained consistent across animals (L1: 41–62% VM; 27–65% VL) (Figure. 16b), with mean values of 51.5% for $V3_{VM}$ and 46% for $V3_{VL}$ (Figure. 16a).

In contrast, the non-stimulated control animal exhibited lower and less segmentally distinct recruitment patterns. Within the L2 segment, of the 35 V3V neurons identified, baseline cFos expression was observed in 9 of 26 (35%) $V3_{VM}$ neurons and 4 of 9 (44%) $V3_{VL}$ neurons, while the 30 V3V neurons identified in the adjacent L1 segment showed 10 of 19 (53%) $V3_{VM}$ and 4 of 11 (36%) $V3_{VL}$ activation. Compared with stimulated animals, the control condition showed reduced, less consistent medial-lateral recruitment, suggesting that ventral root stimulation enhances activity-dependent recruitment above baseline spinal activity levels.

Conversely, L6 stimulation showed a high level of $V3_{VM}$ activation within the targeted L6 segment (73–75%) (Figure. 16b), with a corresponding mean of 74% (Figure. 16a), whereas $V3_{VL}$ activation exhibited greater variability (27–60%, Figure. 16b; mean 43.5%, Figure. 16a). In the adjacent L5 segment, activation patterns were more variable between animals (0–48% VM; 0–91% VL) (Figure. 16b), with mean activation levels of 24% for $V3_{VM}$ and 45.5% for $V3_{VL}$ (Figure. 16a). Interestingly, additional analysis of the more caudal S1 segment in one L6-stimulated animal revealed sustained recruitment of V3V populations, with cFos expression observed in 81% of

$V3_{VM}$ neurons and 58% of $V3_{VL}$ neurons, indicating that caudal stimulation may recruit spinal networks beyond the immediately adjacent lumbar segment. These initial findings suggest that while L2 stimulation produces relatively balanced and consistent recruitment of both medial and lateral V3 subpopulations across local and adjacent segments, L6 stimulation may result in selective activation of $V3_{VM}$ neurons within the stimulated segment, accompanied by reduced medial recruitment and more variable lateral activation in adjacent segments. The presence of cFos activation in the non-stimulated control animal suggests a baseline level of spontaneous or ongoing spinal network activity, whereas the recruitment observed following ventral root stimulation supports activity-dependent engagement of V3V circuits in a segment-specific manner.

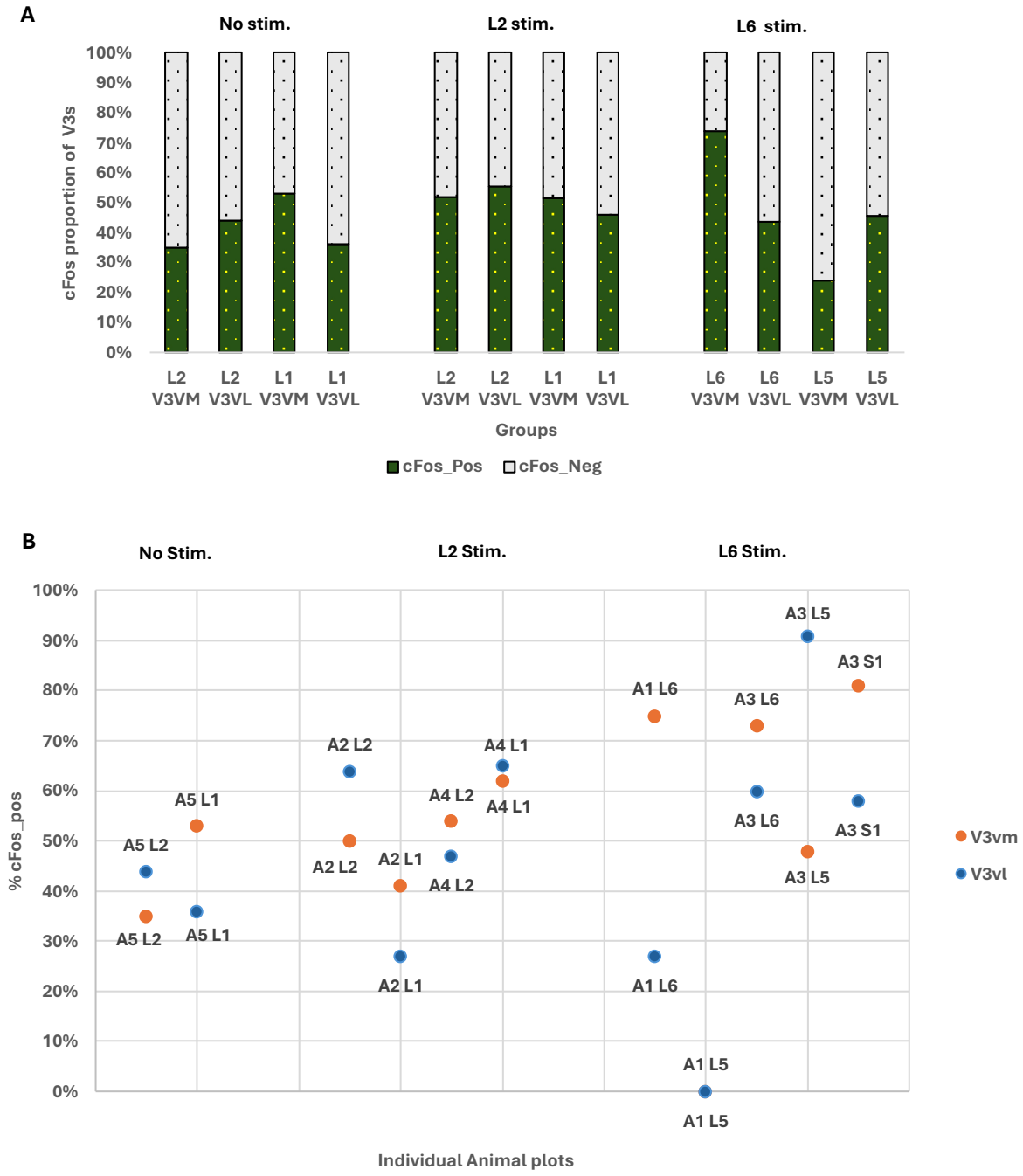

Figure 16: Activity-dependent recruitment of V3V subpopulations following segment-specific ventral root stimulation.
(A) Mean Proportional distribution of cFos-positive and cFos-negative $V3_{VM}$ and $V3_{VL}$ neurons within each analyzed segment of all five Mice in response to L2 and L6 stimulation, and non-stimulation (non-stim, n=1; L2-stim, n=2; L6-stim, n=2) (B) Individual Mouse values showing variability in recruitment patterns across stimulated and non-stimulated segments. Data are

presented as a percentage of the total cFos+ $V3_{VM}$ or $V3_{VL}$ neurons within each analyzed segment.

4.3.1 Supplementary observations of left-right recruitment patterns

To further examine the spatial distribution of cFos activation, V3V subpopulations were analyzed across the left and right sides of the spinal cord in stimulated and non-stimulated mice (Table 2). Although ventral root stimulation was applied unilaterally, the stimulated side was not consistently tracked across all experiments; therefore, observations are described according to left-right hemicord distribution rather than ipsilateral versus contralateral recruitment. Across both L2- and L6-stimulated mice, cFos expression was observed bilaterally within $V3_{VM}$ and $V3_{VL}$ populations. In L2-stimulated mice (mice 2 and 4), activation levels were generally comparable between left and right sides in the L2 and L1 segments, although variability in recruitment was observed between subpopulations and mice. For example, in mouse 2, right-sided L2 $V3_{VL}$ neurons exhibited complete cFos recruitment (100%), whereas left-sided $V3_{VL}$ neurons showed lower activation (50%). Similarly, mouse 4 demonstrated relatively balanced bilateral recruitment within both $V3_{VM}$ and $V3_{VL}$ populations across L1 and L2 segments (42–75%).

L6-stimulated mice also demonstrated bilateral recruitment patterns. In Mouse 3, strong cFos expression was observed on both sides of the stimulated L6 segment within $V3_{VM}$ (72–73%) and $V3_{VL}$ (59–62%) populations. Robust bilateral activation additionally extended into L5 and caudal S1 segments, particularly within $V3_{VL}$ neurons in L5 (86–100%) and $V3_{VM}$ neurons in S1 (79–83%). In contrast, Mouse 1 exhibited more restricted recruitment, with cFos activation largely confined to the L6 segment and absent within L5 populations.

The non-stimulated control mouse also exhibited bilateral baseline cFos expression within both $V3_{VM}$ and $V3_{VL}$ populations. Across the L2 segment, cFos expression was detected in 35%

of $V3_{VM}$ neurons and 44% of $V3_{VL}$ neurons, while the adjacent L1 segment showed cFos expression in 53% of $V3_{VM}$ neurons and 36% of $V3_{VL}$ neurons. In comparison, L2-stimulated mice demonstrated cFos expression ranging from 50-54% in $V3_{VM}$ neurons and 47-64% in $V3_{VL}$ neurons within the stimulated L2 segment, with activation also present in the adjacent L1 segment. These supplementary observations suggest that V3V recruitment following ventral root stimulation is not strictly unilateral, but instead extends bilaterally across spinal hemicords, consistent with the known commissural and intersegmental properties of V3 neuron networks.

Table 2: Left-right distribution of cFos-positive V3V neurons following segment-specific stimulation

Mice	Stimulation	Segment	Side	Sub-population	Total V3s	cFos_pos count	cFos_neg count	cFos_pos%	cFos_neg%
Mouse 1 (f)	L6	L6	Right	V3vm	6	4	2	67%	33%
		L6	Right	V3vl	12	4	8	33%	67%
		L6	Left	V3vm	2	2	0	100%	0%
		L6	Left	V3vl	3	0	3	0%	100%
		L5	Right	V3Vm	2	0	2	0%	100%
Mouse 2 (m)	L2	L2	Right	V3vm	25	12	13	48%	52%
		L2	Right	V3vl	3	3	0	100%	0%
		L2	Left	V3vm	17	9	8	53%	47%
		L2	Left	V3vl	8	4	4	50%	50%
		L1	Right	V3vm	15	8	7	53%	47%
		L1	Right	V3vl	10	1	9	10%	90%
		L1	Left	V3vm	17	5	12	29%	71%
		L1	Left	V3vl	5	3	2	60%	40%
Mouse 3 (m)	L6	L6	Right	V3vm	25	18	7	72%	28%
		L6	Right	V3vl	13	8	5	62%	38%
		L6	Left	V3vm	26	19	7	73%	27%
		L6	Left	V3vl	27	16	11	59%	41%
		L5	Right	V3vm	33	15	18	45%	55%
		L5	Right	V3vl	18	18	0	100%	0%
		L5	Left	V3vm	33	17	16	52%	48%
		L5	Left	V3vl	28	24	4	86%	14%
		S1	Right	V3vm	18	15	3	83%	17%
		S1	Right	V3vl	29	17	12	59%	41%
		S1	Left	V3vm	29	23	6	79%	21%
		S1	Left	V3vl	19	11	8	58%	42%
		L6	Right	V3vm	25	18	7	72%	28%
		L6	Right	V3vl	13	8	5	62%	38%

Mouse 4 (f)	L2	L2	Right	V3vm	14	9	5	64%	36%
		L2	Right	V3vl	5	3	2	60%	40%
		L2	Left	V3vm	23	11	12	48%	52%
		L2	Left	V3vl	12	5	7	42%	58%
		L1	Right	V3vm	20	13	7	65%	35%
		L1	Right	V3vl	8	6	2	75%	25%
		L1	Left	V3vm	19	11	8	58%	42%
		L1	Left	V3vl	12	7	5	58%	42%
		L2	Right	V3vm	14	9	5	64%	36%
Mouse 5 (m)	Non-stim	L2	Right	V3vm	13	6	7	46%	54%
		L2	Right	V3vl	2	0	2	0%	100%
		L2	Left	V3vm	13	3	10	23%	77%
		L2	Left	V3vl	7	4	3	57%	43%
		L1	Right	V3vm	13	6	7	46%	54%
		L1	Right	V3l	5	1	4	20%	80%
		L1	Left	V3vm	6	4	2	67%	33%
		L1	Left	V3v	6	3	3	50%	50%

Chapter V: Discussion

5.1 Overview

This study provides preliminary data regarding the spatial organization, molecular identity, and functional recruitment of V3V IN subpopulations in the adult lumbar spinal cord. We examined the rostrocaudal distribution of ventromedial ($V3_{VM}$) and ventrolateral ($V3_{VL}$) V3 neurons, examined their expression of the projection-associated transcription factors Zfhx3 and NFIB, and their recruitment following segment-specific ventral root stimulation using cFos expression as a marker of neuronal activity. We observed that V3V subpopulations exhibited a rostrocaudal distribution pattern across individual mice, characterized by a predominance of $V3_{VM}$ neurons throughout the lumbar spinal cord and a progressive increase in $V3_{VL}$ representation within the caudal lumbar segments. In addition, both $V3_{VM}$ and $V3_{VL}$ populations expressed Zfhx3 and NFIB, indicating molecular heterogeneity within V3V neurons and suggesting the coexistence of putative long- and short-range projection phenotypes. Lastly, ventral root stimulation recruited both $V3_{VM}$ and $V3_{VL}$ neurons, but the recruitment pattern varied with the stimulated segment, supporting a role for V3V neurons in segment-specific motor network activation. These findings suggest that V3V neurons are spatially organized, molecularly heterogeneous, and functionally recruited in a segment-dependent manner.

5.2 Rostrocaudal Organization of V3V Subpopulations

Across the three mice analyzed, $V3_{VM}$ neurons were the most common V3V population observed throughout the lumbar spinal cord, representing 80% of V3V neurons in L1-L2, 92% in L3-L5, and 63% in L6. Whereas $V3_{VL}$ neurons were present in the rostral lumbar cord, they

became relatively sparse within the mid-lumbar enlargement and increased markedly in the caudal lumbar segment, showing a segment-dependent variation, representing 20% in L1-L2, 8% in L3-L5, and 38% in L6. This demonstrates that the mediolateral distribution of V3V neurons changes significantly along the rostrocaudal lumbar axis. The observation of $V3_{VM}$ neurons within the L3-L5 region is notable because these segments correspond to the lumbar enlargement, which contains neural circuits involved in hindlimb locomotor control. Although the primary rhythm-generating circuitry has been localized to the rostral lumbar spinal cord (approximately T12-L2), the lumbar enlargement contributes importantly to the patterning and execution of locomotor output (Cazalets et al., 1995; Cowley & Schmidt, 1997; Kiehn, 2016; Chopek et al., 2018). Previous studies suggest that $V3_{VM}$ neurons participate in recurrent excitatory networks and may integrate descending and local spinal signals (Chopek et al., 2018). In contrast, the greater representation of $V3_{VL}$ neurons within L1-L2, and particularly in L6, may indicate regional specialization of this subpopulation along the rostrocaudal axis of the lumbar spinal cord. Chopek et al. (2018) demonstrated that $V3_{VL}$ neurons form direct excitatory connections with motoneurons, raising the possibility that the higher proportion of V3 neurons observed in caudal lumbar segments could be associated with increased premotor modulation of distal hindlimb musculature. However, because the present study was descriptive and did not directly examine neuronal connectivity or function, this interpretation remains speculative and warrants further investigation. These findings suggest that the spatial organization of V3V neurons in the lumbar spinal cord may reflect functional specialization along the rostrocaudal axis. Similar segmental specialization has been reported for motoneuron pools, sensory pathways, and locomotor IN networks (McHanwell & Biscoe, 1981; Kiehn, 2016; Laliberte et al., 2019). The present findings further extend the layered microcircuit model proposed by Chopek et al. (2018), in which $V3_{VM}$ neurons function primarily as integrative

elements within recurrent excitatory networks, whereas $V3_{VL}$ neurons act as output-related neurons with direct influence over motoneurons. Within the lumbar segments examined in this study, the increase of $V3_{VM}$ neurons in the lumbar enlargement, together with the relatively greater representation of $V3_{VL}$ neurons in caudal lumbar segments, may suggest that rostrocaudal organization of V3V populations may reflect regional specialization within lumbar spinal circuitry.

5.3 Molecular Heterogeneity of V3V Neurons

Previous developmental studies demonstrated that transcription factor expression can predict projection identity and circuit function within spinal INs (Delile et al., 2019; Osseward et al., 2021). Zfhx3 has been associated with neurons possessing long-range projection characteristics, whereas NFIB has been linked to more locally organized neuronal populations (Hsu et al., 2015; Delile et al., 2019). We observed that subsets of both $V3_{VM}$ and $V3_{VL}$ neurons expressed Zfhx3 and NFIB. However, the Zfhx3 and NFIB immunolabeling were performed on different tissue sections rather than on the same or serial sections, and expression of these transcription factors was quantified independently. Consequently, the reported percentages cannot be interpreted as complementary proportions or used to infer co-expression between the two markers. At L2, approximately 65% of identified $V3_{VM}$ neurons and 85% of identified $V3_{VL}$ neurons were Zfhx3-positive, while at L6, approximately 64% of identified $V3_{VM}$ neurons and 90% of identified $V3_{VL}$ neurons were Zfhx3-positive. For NFIB, approximately 67% of identified $V3_{VM}$ neurons and 52% of identified $V3_{VL}$ neurons at L2 were NFIB-positive, while at L6, approximately 59% of identified $V3_{VM}$ neurons and 65% of identified $V3_{VL}$ neurons expressed NFIB. The observation that substantial proportions of both $V3_{VM}$ and $V3_{VL}$ neurons express these

markers suggests that projection identity does not strictly segregate by mediolateral position. Instead, both populations appear molecularly heterogeneous. Importantly, because Zfhx3 and NFIB were examined in separate tissue sets, the present study cannot determine whether these transcription factors define mutually exclusive neuronal populations or whether individual V3 neurons co-express both markers. Recent transcriptomic studies indicate that spinal IN identity is often defined by combinatorial expression of transcription factors rather than by single-marker classification (Delile et al., 2019; Osseward et al., 2021). Consequently, the observed proportions should be interpreted as evidence that multiple projection-associated molecular phenotypes are present within both $V3_{VM}$ and $V3_{VL}$ populations, rather than as distinct non-overlapping neuronal classes. In addition, Zfhx3 expression appeared particularly enriched within $V3_{VL}$ neurons at L6. Although caution is warranted given sample size limitations, this observation suggests that a subset of caudal $V3_{VL}$ neurons may participate in longer-range propriospinal communication. In contrast, NFIB expression was relatively evenly distributed across $V3_{VM}$ and $V3_{VL}$ populations. This finding suggests that local circuit-associated phenotypes are present throughout V3V populations. Overall, the molecular data indicate that mediolateral position alone does not fully define projection-associated identity within V3V neurons. Instead, both $V3_{VM}$ and $V3_{VL}$ populations appear to contain molecularly diverse subgroups. This supports the broader idea that spinal IN identity is shaped by the interaction between anatomical position, transcription factor expression, and circuit connectivity (Delile et al., 2019; Osseward et al., 2021).

5.4 Functional Recruitment of V3V Neurons Following Ventral Root Stimulation

We observed that ventral root stimulation recruited V3V neuron subpopulations in a segment-dependent manner. Electrical stimulation of ventral roots activates motor axons antidromically, generating action potentials that propagate back toward motoneuron cell bodies and may engage local spinal circuitry through recurrent motor pathways (Eccles, 1955; Kuno, 1959; Lipski, 1981). To minimize sensory contributions, dorsal roots were transected prior to stimulation, ensuring that cFos expression predominantly reflected activation of motor-associated spinal networks. Although both stimulation paradigms recruited V3V neurons, distinct patterns emerged between rostral and caudal lumbar segments. In response to L2 stimulation, cFos expression was relatively balanced between $V3_{VM}$ and $V3_{VL}$ populations within the stimulated segment, with mean recruitment of 52% and 55%, respectively. Recruitment was also observed in the adjacent L1 segment, suggesting that activation of rostral lumbar motor pathways engages V3V circuits beyond the stimulated level. Although cFos expression was observed following ventral root stimulation, comparison with the non-stimulated control; n=1, revealed similar numbers of cFos-positive V3 neurons, particularly following L2 stimulation; n=2. Consequently, the present data do not provide definitive evidence that the observed cFos expression resulted solely from ventral root stimulation and should therefore be interpreted with caution. In contrast, L6 stimulation preferentially recruited $V3_{VM}$ neurons within the stimulated segment, with 74% of $V3_{VM}$ neurons expressing cFos compared with 43% of $V3_{VL}$ neurons. This preferential activation may reflect the proposed role of $V3_{VM}$ neurons as integrative elements within V3V circuitry. Chopek et al. (2018) demonstrated that $V3_{VM}$ neurons participate in recurrent excitatory networks, positioning them to integrate and distribute motor-related signals within the spinal cord. Their extensive local connectivity may therefore make them particularly susceptible to activation

following antidromic stimulation of motor pathways. Recruitment within the adjacent L5 segment was more variable between mice. Notably, one animal exhibited no detectable cFos expression in either $V3_{VM}$ or $V3_{VL}$ neurons, suggesting limitations in our techniques for that animal, whereas another showed cFos labelling, particularly within the $V3_{VL}$ population (Figure 13). This may reflect differences in stimulation duration, because the mouse lacking L5 cFos expression received 60 minutes of ventral root stimulation, whereas the remaining mice received 90 minutes of stimulation before the post-stimulation survival period. Because cFos expression is activity-dependent and influenced by the duration of neuronal activation (Morgan & Curran, 1991; Kovács, 2008), the shorter stimulation period may have been insufficient to generate detectable cFos accumulation in more distant or indirectly recruited circuits. Thus, the absence of L5 activation in this mouse may reflect methodological variation rather than a true absence of intersegmental recruitment. Importantly, cFos expression extended beyond the stimulated segment, including recruitment within adjacent lumbar segments and, in one mouse, the sacral spinal cord (Figure 15). This observation supports the notion that V3V neurons participate in intersegmental spinal networks and is consistent with growing evidence that subsets of V3 neurons contribute to propriospinal communication and the coordination of motor activity across multiple spinal levels (Danner et al., 2019; Zhang et al., 2022). These findings suggest that V3V neurons contribute not only to local premotor circuitry but also to the propagation of motor-related activity throughout the rostrocaudal spinal cord.

An additional observation was bilateral cFos activation following unilateral ventral root stimulation. However, caution should be exercised in over-interpreting this data, given that the stimulated side was not consistently recorded, cFos-positive V3 neurons were observed in both sides of the spinal cord. This finding is consistent with the established commissural nature of V3

neurons, which project across the midline and provide excitatory coupling between the left and right sides of the spinal cord (Zhang et al., 2008; Blacklaws et al., 2015; Chopek et al., 2018). Experimental and computational studies suggest that these commissural connections contribute to locomotor stability, rhythm robustness, and bilateral coordination (Danner et al., 2019; Ausborn et al., 2021). The bilateral recruitment observed in the present study, therefore, supports the involvement of V3V neurons in commissural spinal networks. These findings suggest that recruitment of V3V neurons may be influenced by the segmental location of motor pathway activation. Whereas rostral lumbar stimulation produced relatively balanced recruitment of $V3_{VM}$ and $V3_{VL}$ neurons, caudal stimulation preferentially engaged $V3_{VM}$ neurons and recruited activity across multiple spinal segments. Also, V3V neurons may contribute to both local and intersegmental motor network organization, and their recruitment reflects underlying functional specialization within spinal locomotor circuits. Overall, these findings should be considered preliminary. Although differences in cFos expression were observed following ventral root stimulation, the similar numbers of cFos-labelled V3V neurons in stimulated and non-stimulated animals, particularly after L2 stimulation, together with the limited number of animals and sections analyzed, mean that firm conclusions cannot yet be drawn regarding stimulation-induced recruitment. Rather, these findings provide a basis for further investigation using larger sample sizes, additional controls, and refined stimulation protocols to better understand how ventral root stimulation recruits V3V neuron populations.

5.5 Limitations

A key limitation of this study is that the number of animals included in objectives 2 and 3 were small, which limited statistical power and the ability to detect biological differences. Another limitation is that projection identity was inferred using Zfhx3 and NFIB as putative molecular markers of long- and short-range connectivity. Although this approach is supported by developmental and transcriptomic studies, direct anatomical tracing, such as using horizontal (longitudinal) sectioning of the spinal segments instead of cross-sectional, was not performed and therefore, projection patterns using anatomical tracing were not explored. A third limitation was that neuronal activation was assessed using cFos expression, which provides an indirect measure of activity and cannot distinguish between direct and polysynaptic recruitment. Also, cFos expression in our one control animal was relatively similar to cFos expression in our n = 2 animals that received stimulation at L2, limiting our ability to discern whether our stimulation activated any additional neurons compared to control conditions. Further animals would be needed to understand whether our findings represented actual recurrent activation of V3 Ins or was merely an artifact of background cFos labelling under our experimental conditions. Finally, variability in tissue recovery and section sampling may have contributed to some of the differences observed between animals. Despite these limitations, we did observe a trend in our small sample that suggests consistency across animals, supporting the possibility that a rostrocaudal distribution patterns of V3V subpopulations exists within the lumbar spinal cord. These data provide preliminary evidence for future studies employing anatomical tracing, electrophysiological approaches, and larger sample sizes to further define the connectivity and functional roles of V3V neurons.

Chapter VI: Conclusion

6.1 Key Findings

The findings from this thesis suggests that V3V neurons are organized in a segment-dependent manner along the rostrocaudal axis, with greater numbers of $V3_{VM}$ neurons throughout the lumbar cord (79.7% in L1-L2, 92.3% in L3-L5, and 62.7% in L6), while $V3_{VL}$ neurons were relatively sparse in the mid-lumbar enlargement and increased in caudal lumbar segments (20.3%, 7.7%, and 37.3%, respectively). These observations suggest that V3V subpopulations are spatially specialized and may contribute differently to locomotor and motor control across lumbar segments. In addition to their anatomical organization, both $V3_{VM}$ and $V3_{VL}$ populations exhibited molecular heterogeneity, with gretaer proportions of neurons expressing the projection-associated transcription factors Zfhx3 and NFIB. Functional analyses further revealed segment-dependent recruitment of V3V neurons following ventral root stimulation. Whereas L2 stimulation recruited $V3_{VM}$ and $V3_{VL}$ neurons relatively equally (52.0% and 55.5%, respectively), L6 stimulation preferentially activated $V3_{VM}$ neurons (74.0%) compared with $V3_{VL}$ neurons (43.5%). These findings provide a preliminary investigation of the spatial distribution, molecular identity, and functional recruitment of V3V organization. By extending the current understanding of V3V diversity beyond mediolateral classification, this work identifies a previously unrecognized level of rostrocaudal specialization and lays the foundation for future studies investigating how distinct V3V subpopulations contribute to spinal motor circuit organization and function.

6.2 Future Directions

Future studies can build upon these preliminary findings by further defining the connectivity, molecular diversity, and functional roles of V3V neuron subpopulations. Combining molecular profiling with anatomical tracing approaches would enable direct identification of the projection targets of $V3_{VM}$ and $V3_{VL}$ neurons and help validate the projection-associated identities suggested by Zfhx3 and NFIB expression. In parallel, single-cell transcriptomic analyses could help resolve the molecular heterogeneity of V3V neurons and uncover gene expression associated with distinct $V3_{VM}$ and $V3_{VL}$ phenotypes. These approaches would provide a more comprehensive framework for understanding whether and how molecular identity contributes to the organization and connectivity of V3V circuits.

Building on the preliminary anatomical and molecular findings presented here, ongoing studies in our laboratory will investigate the descending and sensory inputs to $V3_{VM}$ and $V3_{VL}$ neurons, providing an opportunity to determine how these subpopulations are differentially integrated within sensorimotor and supraspinal pathways. Future experiments will also expand upon the ventral root stimulation paradigm by combining activity-dependent mapping with electrophysiological recordings to confirm whether differential recruitment patterns can be observed through cFos expression, and whether any patterns observed correspond to distinct synaptic properties, connectivity profiles, and circuit functions. These studies will increase our understanding of how V3V subpopulations contribute to the integration of sensory, descending, and motor-related signals within spinal locomotor networks.

Ultimately, understanding the anatomical, molecular, and functional specialization of V3V neurons may provide important insight into the principles governing spinal circuit organization.

Extending these investigations to spinal cord injury models could further reveal whether specific V3V subpopulations contribute to circuit reorganization, locomotor recovery, or maladaptive motor outcomes, such as spasticity. Such studies have the potential to identify V3V neurons as important cellular substrates for both normal motor control and therapeutic interventions to restore function after neurological injury.

References

- Alaynick, W. A., Jessell, T. M., & Pfaff, S. L. (2011). *Spinal cord development*. Cell, 146(1), 178-178.e1.
- Allen Institute for Brain Science. (2011). *Allen Mouse Brain Atlas*. Seattle, WA: Allen Institute for Brain Science.
- Bikoff et al. (2016). *Spinal inhibitory IN diversity delineates variant motor microcircuits.*
- Blacklaws, J., Deska-Gauthier, D., Jones, C. T., Petracca, Y. L., Liu, M., Zhang, H., Fawcett, J. P., Glover, J. C., & Zhang, Y. (2015). Sim1 is required for the migration and axonal projections of V3 INs in the developing mouse spinal cord. *Developmental Neurobiology*, 75(9), 1003-1017.
- Borowska, J., Jones, C. T., Zhang, H., & Zhang, Y. (2013). Functional subpopulations of V3 INs in the mature mouse spinal cord. Journal of Neuroscience, 33, 18553 to 18565.
- Borowska, J., Kirby, A., & Zhang, Y. (2015). Postnatal maturation of V3 IN subpopulations in the mouse spinal cord. *Neuroscience*, 293, 34 to 47.
- Bouyer, L. J., & Rossignol, S. (2003). Contribution of cutaneous inputs from the hindpaw to the control of locomotion. I. Intact cats. *Journal of Neurophysiology*, 90(6), 3625-3639.
- Brown, T. G. (1911). The intrinsic factors in the act of progression in the mammal. *Proceedings of the Royal Society of London. Series B, Containing Papers of a Biological Character*, 84(572), 308-319.
- Brown, T. G. (1914). On the nature of the fundamental activity of the nervous centres; together with an analysis of the conditioning of rhythmic activity in progression, and a theory of the evolution of function in the nervous system. *The Journal of Physiology*, 48(1), 18-46.
- Brownstone, R., & Chopek, J. W. (2018). Reticulospinal systems for tuning motor commands. *Journal of Neurophysiology*, 120, 1767 to 1780.
- Carr, P. A., Huang, A., Noga, B. R., & Jordan, L. M. (1995). CFos expression in cat spinal neurons during fictive locomotion induced by the mesencephalic locomotor region. *Journal of Neurophysiology*, 73(2), 646-658.
- Cazalets, J. R., Sqalli-Houssaini, Y., & Clarac, F. (1992). *A*ctivation of the central pattern generators for locomotion by serotonin and excitatory amino acids in neonatal rat. The *Journal of Physiology*, 455, 187-204.
- Chacon C, Nwachukwu CV, Shahsavani N, Cowley KC and Chopek JW (2023) Lumbar V3 INs provide direct excitatory synaptic input onto thoracic sympathetic preganglionic neurons, linking locomotor, and autonomic spinal systems. *Front. Neural Circuits* 17:1235181. doi: 10.3389/fncir.2023.1235181
- Chopek JW, Nascimento F, Beato M, Brownstone RM, Zhang Y. (2018). *F*unctional specialization of V3 INs in locomotor control. *Cell Reports*, 23, 3022-3034.

- Cowley, K. C., & Schmidt, B. J. (1997). *R*egional distribution of the locomotor pattern-generating network in the neonatal rat spinal cord. *Journal of Neurophysiology*, 77, 247-259.
- Cowley, K. C., Zaporozhets, E., & Schmidt, B. J. (2008). Propriospinal neurons are sufficient for brainstem-evoked locomotor-like activity in the in vitro neonatal rat spinal cord. *Journal of Neurophysiology.*
- Crone, S. A., Quinlan, K. A., Zagoraiou, L., Droho, S., Restrepo, C. E., Lundfald, L., Endo, T., Setlak, J., Jessell, T. M., Kiehn, O., & Sharma, K. (2008). Genetic ablation of V2a ipsilateral INs disrupts left-right locomotor coordination in mammalian spinal cord. *Neuron,* 60(1), 70-83.
- Danner, S. M., Shevtsova, N. A., Frigon, A., & Rybak, I. A. (2019). Computational modeling of spinal circuits controlling limb coordination and gaits in quadrupeds. *eLife*, 8, e31050.
- Danner, S. M., Zhang, H., Shevtsova, N. A., Borowska, J., Rybak, I. A., & Zhang, Y. (2019). Spinal V3 INs and left-right coordination in mammalian locomotion. *Frontiers in Cellular Neuroscience*, 13, 516.
- Delile, J., Rayon, T., Melchionda, M., Edwards, A., Briscoe, J., & Sagner, A. (2019). Single cell transcriptomics reveals spatial and temporal dynamics of gene expression in the developing mouse spinal cord. *Development,* 146(12), dev173807.
- Deska Gauthier, D., Roy, R., & Zhang, Y. (2020). Temporal neurogenesis patterning of p3 derived V3 INs. *Journal of Neuroscience*, 40, 1440 to 1452.
- Deska Gauthier, D., Vaidya, M., & Zhang, Y. (2024). Embryonic temporal spatial delineation of excitatory spinal V3 IN diversity. *Cell Reports*, 113, 112420.
- Deska-Gauthier, D., & Zhang, Y. (2019). The functional diversity of spinal commissural INs in locomotor control. *Frontiers in Neural Circuits*, 13, 87.
- Eccles JC. (1955). The central action of antidromic impulses in motor nerve fibres. *Pflügers Archiv*, 260, 385-415.
- Flynn, J. R., Graham, B. A., Galea, M. P., & Callister, R. J. (2011). *T*he role of propriospinal INs in recovery from spinal cord injury. *Neuropharmacology*, 60(5), 809-822.
- Francius, C., Harris, A., Rucchin, V., Hendricks, T. J., Stam, F. J., Barber, M., Kurek, D., Campbell, K., Erdman, S., & Clotman, F. (2013). Identification of multiple subsets of ventral INs and differential distribution along the rostrocaudal axis of the developing spinal cord. *PLoS ONE,* 8(8), e70325.
- Gosgnach, S., Lanuza, G. M., Butt, S. J. B., Saueressig, H., Zhang, Y., Velasquez, T., Riethmacher, D., Callaway, E. M., Kiehn, O., & Goulding, M. (2006). *V*1 spinal neurons regulate the speed of vertebrate locomotor outputs. *Nature, 440*(7081), 215-219.
- Gosgnach, S., Bikoff, J. B., Dougherty, K. J., El Manira, A., Lanuza, G. M., & Zhang, Y. (2017). Delineating the diversity of spinal INs in locomotor circuits. *Journal of Neuroscience,* 37(45), 10835-10841.

- Grillner, S. (1985). Neurobiological bases of rhythmic motor acts in vertebrates. *Science*, 228(4696), 143-149.
- Herrera DG, Robertson HA. (1996). Activation of cFos in the nervous system. *Progress in Neurobiology*, 50, 83-107.
- Jankowska, E. (1992). Interneuronal relay in spinal pathways from proprioceptors. *Progress in Neurobiology,* 38(4), 335-378.
- Jankowska, E. (2001). Spinal Interneuronal systems: Identification, multifunctional character and reconfigurations in mammals. *The Journal of Physiology*, 533(Pt 1), 31-40.
- Jankowska, E. (2008). Spinal Interneuronal networks in the cat: elementary components. *Brain Research Reviews,* 57(1), 46-55.
- Jensen VN, Alilain WJ and Crone SA (2020) Role of Propriospinal Neurons in Control of Respiratory Muscles and Recovery of Breathing Following Injury. *Front. Syst. Neurosci.* 13:84.
- Jessell, T. M. (2000). Neuronal specification in the spinal cord: inductive signals and transcriptional codes. *Nature Reviews Genetics,* 1(1), 20-29.
- Kandel ER, Koester JD, Mack SH, Siegelbaum SA. (2021). *Principles of Neural Science* (6th ed.).
- Kiehn, O. (2006). Locomotor circuits in the mammalian spinal cord. *Annual Review of Neuroscience*, 29, 279-306.
- Kiehn, O. (2016). Decoding the organization of spinal circuits that control locomotion. *Nature Reviews Neuroscience,* 17(4), 224-238.
- Kovács KJ. (1998). cFos as a transcription factor. *Neurochemical International*, 33, 287-297.
- Kudo, N., & Yamada, T. (1987). N-methyl-D,L-aspartate-induced locomotor activity in a spinal cord-hindlimb muscles preparation of the newborn rat studied in vitro. *Neuroscience Letters*, 75(1), 43-48.
- Kuno M. (1959). Excitability changes of spinal motoneurones following antidromic stimulation. *Journal of Physiology*, 149, 374-393.
- Laliberte, A. M., Goltash, S., Lalonde, N. R., & Bui, T. V. (2019). *P*ropriospinal neurons: Essential elements of locomotor control in the intact and possibly the injured spinal cord. *Frontiers in Cellular Neuroscience*, 13, 512.
- Lanuza, G. M., Gosgnach, S., Pierani, A., Jessell, T. M., & Goulding, M. (2004). Genetic identification of spinal INs that coordinate left-right locomotor activity necessary for walking movements. *Neuron*, 42(3), 375-386.
- Lin S, Hari K, Black S, Khatmi A, Fouad K, Gorassini MA, Li Y, Lucas-Osma AM, Fenrich KK, Bennett DJ. Locomotor-related propriospinal V3 neurons produce primary afferent depolarization and modulate sensory transmission to motoneurons. *J Neurophysiol.* 2023 Oct 1;130(4):799-823. doi: 10.1152/jn.00482.2022. Epub 2023 Aug 23. PMID: 37609680; PMCID: PMC10650670.

- Lin, F., & Yang, J. F. (2011). Participation of spinal circuits in locomotor adaptation and recovery after injury. *Experimental Neurology*, 229(2), 241-249.
- Lipski J. (1981). Antidromic activation of neurones as an analytical tool. *Neuroscience Research*, 4, 1-32.
- Martyn Goulding, M. (2009). Circuits controlling vertebrate locomotion: moving in a new direction. *Nature Reviews Neuroscience*, 10(7), 507-518.
- Matsuyama, K., Mori, F., Nakajima, K., Drew, T., Aoki, M., & Mori, S. (2004). Locomotor role of the corticoreticular-reticulospinal-spinal Interneuronal system. *Progress in Brain Research,* 143, 239-249.
- McHanwell, S., & Biscoe, T. J. (1981). The localization of motoneurons supplying the hindlimb muscles of the mouse. *Philosophical Transactions of the Royal Society* B, 293, 477-508.
- Mentis, G. Z., Alvarez, F. J., Bonnot, A., Richards, D. S., Gonzalez-Forero, D., Zerda, R., & O'Donovan, M. J. (2005). Noncholinergic excitatory actions of motoneurons in the neonatal mammalian spinal cord. *Proceedings of the National Academy of Sciences,* 102(20), 7344-7349.
- Morgan JI, Curran T. (1991). Stimulus-transcription coupling in neurons. *Annual Review of Neuroscience*, 14, 421-451.
- Mori, S. (1987). Integration of posture and locomotion in acute decerebrate cats and in awake freely moving cats. *Progress in Neurobiology*, 28(3), 161-195.
- O'Donovan, M. J., Pinter, M. J., & Dum, R. P. (1985). Characteristics of recurrent excitatory postsynaptic potentials produced by motoneuron activation in the neonatal rat spinal cord. *Journal of Neurophysiology*, 54(4), 871-881.
- Osseward, P. J., Amin, N. D., Moore, J. D., Temple, B. A., Barriga, B. K., Bachmann, L. C., Beltran, F., Gullo, M., Clark, M. V., Driscoll, S. P., et al. (2021). Divergent transcriptional programs regulate medial versus lateral V3 IN cell fate and connectivity. *Neuron*, 109(15), 2477-2494.e8.
- Pearson, K. G. (2004). Generating the walking gait: Role of sensory feedback. *Progress in Brain Research*, 143, 123-129.
- Peterson, B. W. (1979). Reticulospinal projections to spinal motor nuclei. *Annual Review of Physiology*, 41, 127-140.
- Purves, D., Augustine, G. J., Fitzpatrick, D., Hall, W. C., LaMantia, A. S., Mooney, R. D., Platt, M. L., & White, L. E. (2018). *Neuroscience* (6th ed.). Oxford University Press.
- Quinlan KA, Kiehn O. (2007). Segmental organization of locomotor networks. *Journal of Neuroscience*, 27, 10645-10655.
- Romanes, G. J. (1964). The motor pools of the spinal cord. *Progress in Brain Research, 11, 93-119.*
- Rossignol, S., Dubuc, R., & Gossard, J. P. (2006). Dynamic sensorimotor interactions in locomotion. *Physiological Reviews*, 86(1), 89-154.

- Rybak, I. A., Dougherty, K. J., & Shevtsova, N. A. (2015). Organization of the mammalian locomotor CPG: Review of computational model and circuit architectures based on genetically identified spinal INs. *eNeuro, 2*(5), ENEURO.0069-15.2015.
- Rybak, I. A., Shevtsova, N. A., Lafreniere-Roula, M., & McCrea, D. A. (2013). Modelling spinal circuitry involved in locomotor pattern generation: Insights from deletions during fictive locomotion. *The Journal of Physiology, 591*(17), 4177-4195.
- Sagner, A., Gaber, Z. B., Delile, J., Kong, J. H., Rousso, D. L., Pearson, C. A., Weicksel, S. E., Melchionda, M., Mousavy Gharavy, S. N., Briscoe, J., & Novitch, B. G. (2021). Olig2 and Hes regulatory dynamics during motor neuron and oligodendrocyte differentiation in the spinal cord. *Developmental Cell*, 56(15), 2151-2168.
- Schubert, D., Kötter, R., Luhmann, H. J., & Staiger, J. F. (2007). Morphology, electrophysiology and functional input connectivity of pyramidal neurons characterized by laminar position in the rat vibrissal cortex. *Cerebral Cortex,* 17(4), 813-836.
- Sherrington, C. S. (1906). The Integrative Action of the Nervous System. *New Haven, CT*: Yale University Press.
- Shevtsova, N. A., Talpalar, A. E., Markin, S. N., Harris-Warrick, R. M., Kiehn, O., & Rybak, I. A. (2015). Organization of left-right coordination of neuronal activity in the mammalian spinal cord: Insights from computational modelling. *Journal of Physiology*, 593(11), 2403-2426.
- Shihao Lin, Yaqing Li, Ana M. Lucas-Osma, Krishnapriya Hari, Marilee J. Stephens, Rahul Singla, C. J. Heckman, Ying Zhang, Karim Fouad, Keith K. Fenrich, and David J. Bennett. Locomotor-related V3 INs initiate and coordinate muscles spasms after spinal cord injury. *Journal of Neurophysiology* 2019 121:4, 1352-1367 10.1152/jn.00776.2018
- Talpalar, A. E., Bouvier, J., Borgius, L., Fortin, G., Pierani, A., & Kiehn, O. (2013). Dual-mode operation of neuronal networks involved in left-right alternation. *Nature*, 500(7460), 85-88.
- Varejão, A. S. P., & Filipe, V. M. (2007). Functional assessment of locomotor recovery after spinal cord injury. *Experimental Neurology*, 203(2), 345-356.
- Wutzke, C. J., Mercer, A., & Graham, B. A. (2013). Intrinsic properties and synaptic connectivity of spinal INs involved in locomotor control. *Journal of Neurophysiology*, 110, 1524-1537.
- Zagoraiou, L., Akay, T., Martin, J. F., Brownstone, R. M., Jessell, T. M., & Miles, G. B. (2009). A cluster of cholinergic premotor INs modulates mouse locomotor activity. *Neuron*, 64(5), 645-662.
- Zhang, H., Xiao, X., & Zhang, Y. (2025). Widespread innervation of motoneurons by spinal V3 INs globally amplifies locomotor output. *Cell Reports*, 42, 114847.
- Zhang, H., Xiao, X., Rotterman, T. M., & Zhang, Y. (2022). V3 neurons coordinate speed-dependent interlimb coupling during locomotion. *eLife*, 11, e73424.

- Zhang, Y., Narayan, S., Geiman, E., Lanuza, G. M., Velasquez, T., Shanks, B., Akay, T., Dyck, J., Pearson, K., Gosgnach, S., & Goulding, M. (2008). V3 spinal neurons establish a robust and balanced locomotor rhythm during walking. *Cell*, 135(1), 84-96.